

Appunti & trasparenze - Parte 6

Versione 3, Novembre 2004

Francesco Fuso, tel 0502214305, 0502214293 - fuso@df.unipi.it

<http://www.df.unipi.it/~fuso/dida>

Sistemi mesoscopici, nanostrutture isolate, ancorate e in matrice: preparazione e proprietà di nanoclusters e nanofili; nanostrutture di carbonio e nanotubi: sintesi, proprietà strutturali e funzionali (elettroniche e meccaniche); esempi di nanocompositi e cenni su proprietà nanomeccaniche

11/11/2004 ITI M 9.30+1

15/11/2004 ITI M 9.30+1

Introduzione

Sistemi **mesoscopici**: sistemi isolati (o ancorati) con dimensioni sub-microscopiche (ma “super-molecolari”) in due o tre dimensioni:

- Nanoclusters (nanoaggregati con numero di unità elementari ~ 100-10000, typ.)
- Nanofili e nanotubi (strutture 1D “piene” o “vuote”)

Generalmente: proprietà fisiche “intermedie” tra bulk e sistemi con confinamento quantico, dipendenti da **dimensioni e geometria**

Comportamento elettronico, strutturale, funzionale (es., trasporto, meccanica, etc.): spesso particolare, anche se non totalmente quantistico.

Metodi di preparazione: estremamente vari (soprattutto fisici e fisico-chimici, cioè non in soluzione)

Applicazioni: molto varie, spesso richiedono ancoraggio o presenza di matrici (**nanocompositi**)

Alcuni metodi di preparazione di nanoclusters

Table 3.2. Methods for cluster generation

a) Condensation of atoms (supersaturation in vapor, liquids, solids)		
Atoms produced by heating: resistive, laser or electron beam		
sputtering: by photon, atom, molecule, or ion impact, electric pulses, electric discharges		
In beams	On surfaces	In matrices
<i>Continuous:</i>		
<ul style="list-style-type: none"> • gas aggregation • adiabatic expansion (with/without carrier gas) • field emission (liquid-metal sources) • spraying techniques 	<ul style="list-style-type: none"> • atom deposition with subsequent surface diffusion • soft landing 	<ul style="list-style-type: none"> • co-evaporation of atoms with matrix material (matrix isolation) • diffusion in/into matrix • photoreduction (photographic material) • spraying techniques into liquid matrix (solvent extraction)
<i>Pulsed:</i>		
<ul style="list-style-type: none"> • laser vaporization • pulsed nozzles for carrier gas 		<ul style="list-style-type: none"> • chemical reduction in liquids (with or without nuclei): colloid generation metalloorganic compounds: ligand shells
b) Dispersion of bulk material or deposition		
<ul style="list-style-type: none"> • sputtering • electric pulses, exploding wire • arc discharges (Svedberg) • laser vaporization, ablation 	<ul style="list-style-type: none"> • cluster deposition from cluster beam • nanocrystalline material by densification 	<ul style="list-style-type: none"> • co-evaporation of clusters with matrix material • arc discharges in liquids • pressing into porous matrix • chemical reduction in zeolites • dispersion by ultrasound (emulsions)

Clusters: sistemi (mesoscopici) composti da un numero relativamente basso di componenti elementari (es., atomi o molecole)

Possono avere comportamento “nanocristallino” o no (es.: carattere metallico? Proprietà ottiche?)

Studi di carattere fondamentale o applicazioni (catalizzatori, sensori, lubrificanti, sistemi meccanici, appl. biomediche, etc.)

Molteplici metodi di preparazione (typ. metodi fisici), es.:

- condensazione di componenti elementari
- frammentazione di bulk

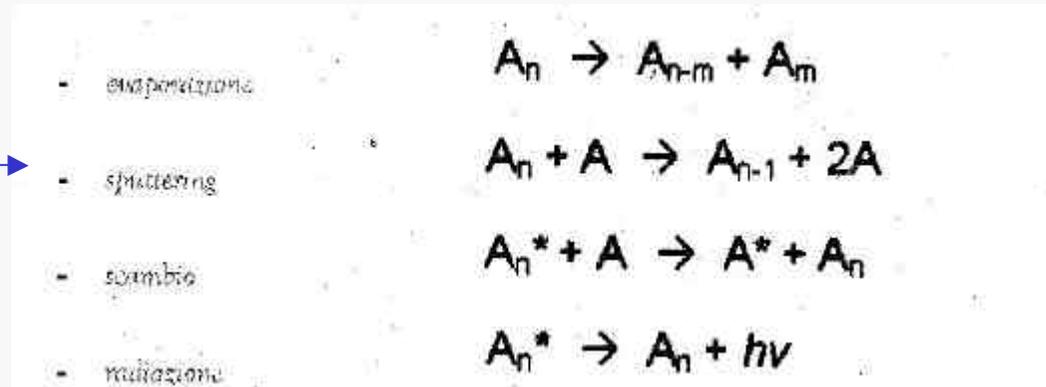
Materiale tratto dal seminario di Giovanni Barcaro, luglio 2003

Stabilizzazione dei nanoclusters

Dal punto di vista termodinamico la crescita di nanoclusters per condensazione è generalmente esotermica → necessità *sottrarre calore*

Alcune reazioni (in fase gassosa) che possono sottrarre calore (da stati eccitati, *):

Oppure buffer-gas che raffredda (espansione supersonica)



Oppure metodi in soluzione (es. precursori metallici idrosolubili per sol. colloidali)

Inoltre c'è possibilità di autoaggregazione (coalescenza) di più nanoclusters (in fase liquida o depositati su substrato)

→ necessità *separare clusters* (es.: con SAM, o con matrici amorfe) o di sfruttare difetti superficiali del substrato (generalmente associati a cicli termici) per indurre la crescita di islands

Inoltre clusters possono essere instabili (*metastabili*)

→ produzione clusters in matrici oppure clusters con **numeri magici**

Tecniche di deposizione di film possono essere "perturbate" per creare clusters

Nanoclusters filamentari (nanofili)

Interesse per nanoclusters in forma filamentare (**nanofili**):

- proprietà di trasporto (sistemi 1DEG, electron waveguides,...)
- proprietà **meccaniche** (flessibilità della struttura, effetti dovuti alle dimensioni nanometriche - *proprietà meccaniche “quantizzate”*)

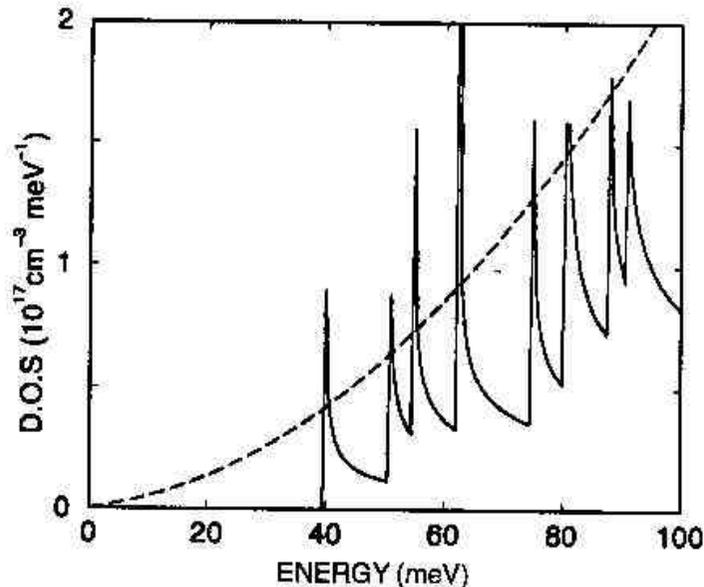


FIG. 15. Calculated effective densities of states for 40-nm bismuth nanowires (solid curve) and bulk bismuth (dashed curve). The zero energy refers to the band edge of bulk bismuth. The nonparabolic effects of the electron carriers are considered in these calculations.

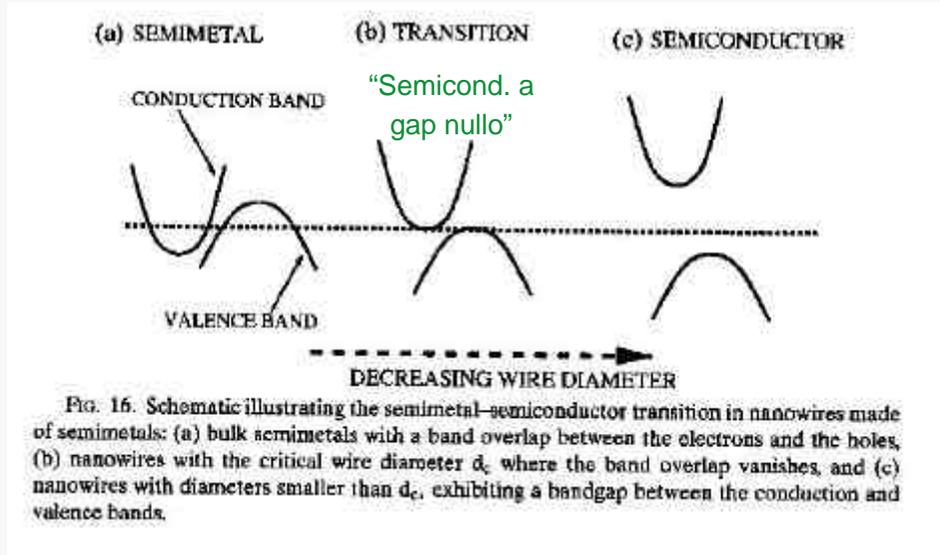
Effetti di confinamento **come in fili quantici**
(per nanofili di diametro nanometrico)

Proprietà elettroniche
dettate da
confinamento (DOS
1DEG)

Ying, Nanostructured
Materials (Academic, 2001)

Proprietà di trasporto e meccaniche di nanofili

Transizione semimetallo->semiconduttore



Dipendenza conducibilità/temperatura

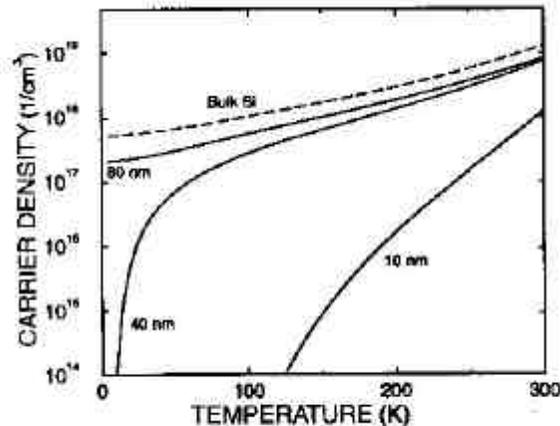
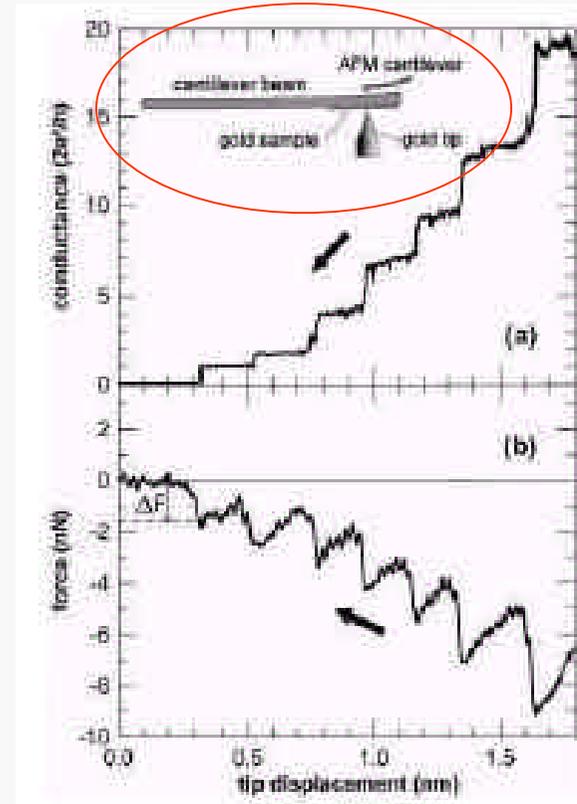


FIG. 17. Calculated total carrier density (electrons and holes) as a function of temperature for bulk 3D bismuth and bismuth nanowires of different diameters oriented along the [0112] direction.

Forza di coesione "quantizzata"



Sistemi con elevata sensibilità
a T, ad adsorbati, a
perturbazioni meccaniche

nanosensoristica

Fabbricazione di nanofili da templates

“Nano-pressofusione” (o estrusione)

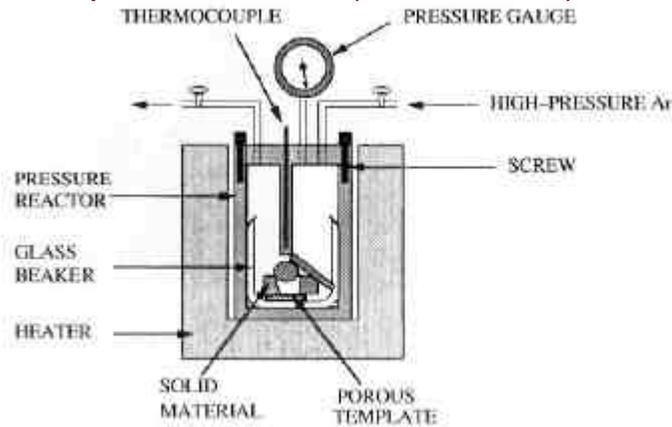


FIG. 5. Schematic of the experimental setup for the pressure injection of materials into the nanochannels of a porous template.

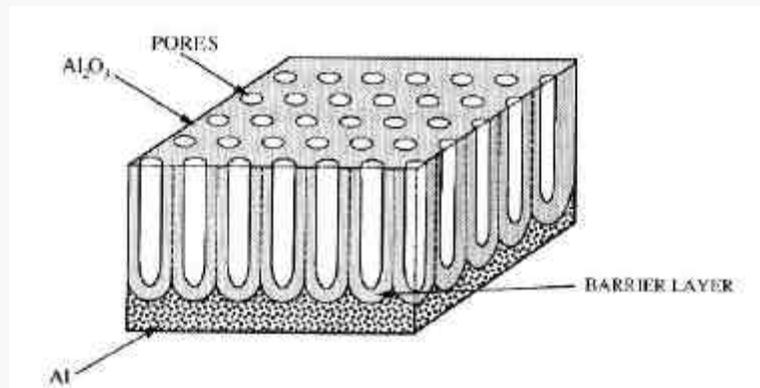


FIG. 1. Schematic of a porous anodic alumina template.

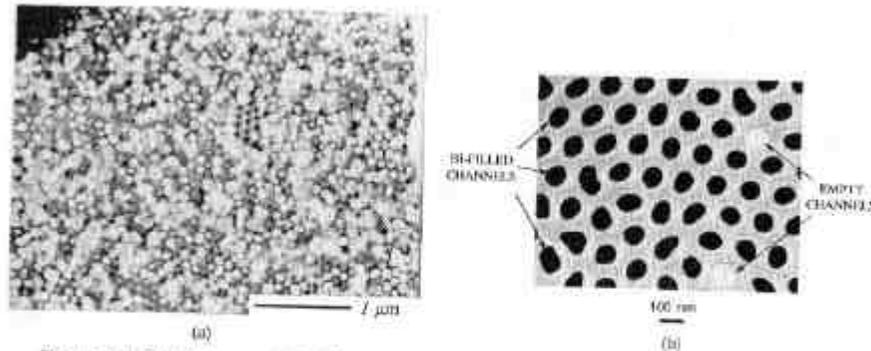


FIG. 6. (a) SEM image of the bottom surface of an anodic alumina template filled with bismuth. The pore diameter is 42 nm. (b) TEM micrograph of the cross section of a 65-nm bismuth nanowire array (Zhang *et al.*, 1999).

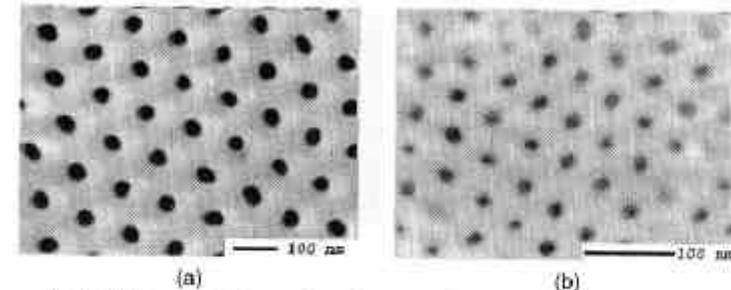


FIG. 2. SEM images of the top surfaces of porous anodic alumina templates anodized in (a) 4 wt% $H_2C_2O_4$ and (b) 20 wt% H_2SO_4 . The average pore diameters in (a) and (b) are 44 nm and 18 nm, respectively.

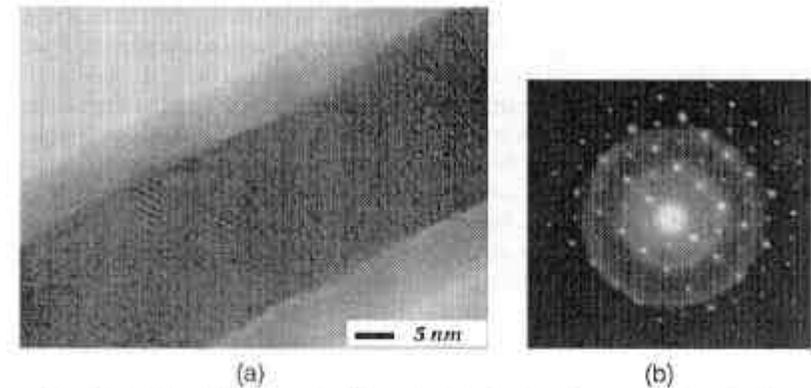


FIG. 7. (a) A HRTEM image of a 40-nm freestanding bismuth nanowire, showing lattice fringes. The amorphous surface layer is bismuth oxide formed upon air exposure of bismuth nanowire. (b) SAED pattern of a single Bi nanowire (Zhang *et al.*, 1999).

Metodi termomeccanici conducono a nanofili cristallini omogenei con metalli (specialmente basso-fondenti)
Dimensioni mesoscopiche

Altri metodi di fabbricazione per nanofili I

Material	Growth Technique	Reference
Ag	DNA-templated, redox template, pulsed ECD ^a	[4.23] [4.24]
Au	template, ECD ^a	[4.25, 26]
Bi	stress-induced	[4.27]
	template, vapor-phase	[4.28]
	template, ECD ^a	[4.29], [4.30], [4.31]
	template, pressure injection	[4.32], [4.16, 33]
Bi ₂ Te ₃	template, dc ECD ^a	[4.34]
CdS	liquid-phase (surfactant), recrystallization	[4.35]
	template, ac ECD ^a	[4.36], [4.37]
CdSe	liquid-phase (surfactant), redox	[4.38]
	template, ac ECD ^a	[4.39], [4.40]
Cu	vapor deposition	[4.41]
	template, ECD ^a	[4.42]
Fe	template, ECD ^a	[4.15], [4.43]
	shadow deposition	[4.44]
GaN	template, CVD ^a	[4.45]
	VLS ^b	[4.46, 47]
GaAs	template, liquid/vapor OMCVD ^d	[4.48]
Ge	high-T, high-P liquid-phase, redox	[4.49]
	VLS ^b	[4.50]
	oxide-assisted	[4.51]
InAs	template, liquid/vapor OMCVD ^d	[4.48]
InP	VLS ^b	[4.52]
Mo	step decoration, ECD ^a + redox	[4.53]
Ni	template, ECD ^a	[4.22], [4.31, 54]
PbSe	liquid phase	[4.55]
Pd	step decoration, ECD ^a	[4.56]
Se	liquid-phase, recrystallization	[4.57]
	template, pressure injection	[4.58]
Si	VLS ^b	[4.59]
	laser-ablation VLS ^b	[4.60]
	oxide-assisted	[4.61]
	low-T VLS ^b	[4.62]
Zn	template, vapor-phase	[4.63]
	template, ECD ^a	[4.64]
ZnO	VLS ^b	[4.65]
	template, ECD ^a	[4.64, 66]

^a Electrochemical deposition
^b Vapor-liquid-solid growth
^c Chemical vapor deposition
^d Organometallic chemical vapor deposition

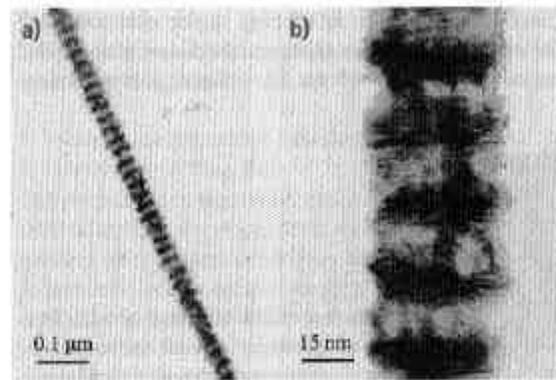


Fig. 4.4 (a) TEM image of a single Co(10 nm)/Cu(10 nm) multilayered nanowire. (b) A selected region of the sample at high magnification [4.76]

Electrochemical Deposition

The electrochemical deposition technique has attracted increasing attention as an alternative method for fabricating nanowires. Traditionally, electrochemistry has been used to grow thin films on conducting surfaces. Since electrochemical growth is usually controllable in the direction normal to the substrate surface, this method can be readily extended to fabricate 1-D or 0-D nanostructures, if the deposition is confined within the pores of an appropriate template. In the electrochemical methods, a thin conducting metal film is first coated on one side of the porous membrane to serve as the cathode for electroplating. The length of the deposited nanowires can be controlled by varying the duration of the electroplating process. This

method has been used to synthesize a wide variety of nanowires e.g., metals (Bi [4.21, 29]; Co [4.73, 74]; Fe [4.15, 75]; Cu [4.20, 76]; Ni [4.22, 73]; Ag [4.24, 77]; Au [4.25, 26]); conducting polymers [4.7, 29]; superconductors (Pb [4.78]); semiconductors (CdS [4.37]); and even superlattice nanowires with A/B constituents (such as Cu/Co [4.20, 76]) have been synthesized electrochemically (see Table 4.1).

In the electrochemical deposition process, the chosen template has to be chemically stable in the electrolyte during the electrolysis process. Cracks and defects in the templates are detrimental to the nanowire growth, since the deposition processes primarily occur in the more accessible cracks, leaving most of the nanopores unfilled. Particle track-etched mica films or polymer membranes are typical templates used in the simple dc electrolysis. To use anodic aluminum oxide films in the dc electrochemical deposition, the insulating barrier layer that separates the pores from the bottom aluminum substrate has to be removed, and a metal film is then evaporated onto the back of the template membrane [4.79]. Compound nanowire arrays, such as Bi₂Te₃, have been fabricated in alumina templates with a high filling factor using the dc electrochemical deposition [4.34]. Figures 4.3a and b, respectively, show the top view and cross-sectional SEM images of a Bi₂Te₃ nanowire array [4.34]. The light areas are associated with Bi₂Te₃ nanowires, the dark regions denote empty pores, and the surrounding gray matrix is alumina.

Surfactants are also used with electrochemical deposition when necessary. For example, when using templates derived from PMMA/PS diblock copolymers (see above), methanol is used as a surfactant is used to facilitate pore filling [4.71], thereby achieving ~ 100% filling factor.

Deposizione elettrochimica
 “attraverso” il template

Da B. Bhushan Ed., Springer Handbook of Nanotechnology (Springer, 2004)

Altri esempi di nanofili

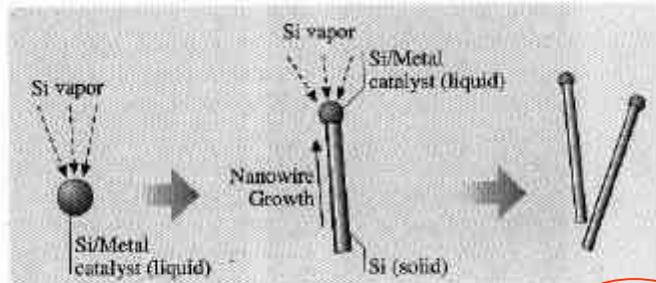


Fig. 4.5 Schematic diagram illustrating the growth of silicon nanowires by the VLS mechanism

4.1.2 VLS Method for Nanowire Synthesis

Some of the recent successful syntheses of semiconductor nanowires are based on the so-called vapor-liquid-solid (VLS) mechanism of anisotropic crystal growth. This mechanism was first proposed for the growth of single crystal silicon whiskers 100 nm to hundreds of microns in diameter [4.87]. The proposed growth mechanism (see Fig. 4.5) involves the absorption of source material from the gas phase into a liquid droplet of catalyst (a molten particle of gold on a silicon substrate in the original work [4.87]). Upon supersaturation of the liquid alloy, a nucleation event generates a solid precipitate of the source material. This seed serves as a preferred site for further deposition of material at the interface of the liquid droplet, promoting the elongation of the seed into a nanowire or a whisker, and suppressing further nucleation events on the same catalyst. Since the liquid droplet catalyzes the incorporation of material from the gas source to the growing crystal, the deposit grows anisotropically as a whisker whose diameter is dictated by the diameter of the liquid alloy

Ruolo catalizzatori nella crescita di nanostrutture

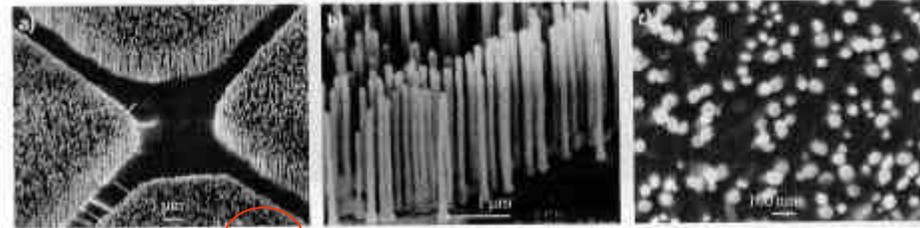


Fig. 4.11a-c SEM images of ZnO nanowire arrays grown on a sapphire substrate, where (a) shows patterned growth, (b) shows a higher-resolution image of the parallel alignment of the nanowires, and (c) shows the faceted side-walls and the hexagonal cross section of the nanowires. For nanowire growth, the sapphire substrates were coated with a 1.0 to 3.5 nm thick patterned layer of Au as the catalyst, using a TEM grid as the shadow mask. These nanowires have been used for nanowire laser applications [4.115]

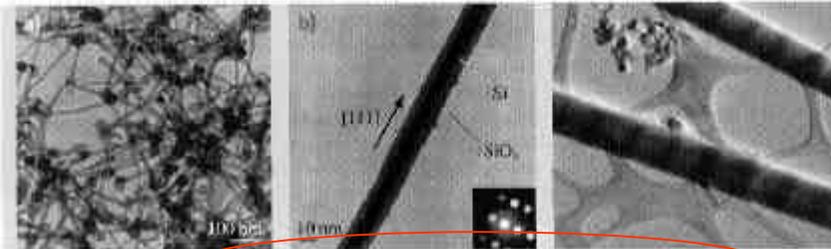


Fig. 4.6 (a) TEM images of Si nanowires produced after laser ablating a $\text{Si}_3\text{O}_2/\text{Fe}_{0.1}$ target. The dark spheres with a slightly larger diameter than the wires are solidified catalyst clusters [4.60]. (b) Diffraction contrast TEM image of a Si nanowire. The crystalline Si core appears darker than the amorphous oxide surface layer. The inset shows the convergent beam electron diffraction pattern recorded perpendicular to the wire axis, confirming the nanowire crystallinity [4.60]. (c) STEM image of $\text{Si}/\text{Si}_{1-x}\text{Ge}_x$ superlattice nanowires in the bright field mode. The scale bar is 500 nm [4.90]

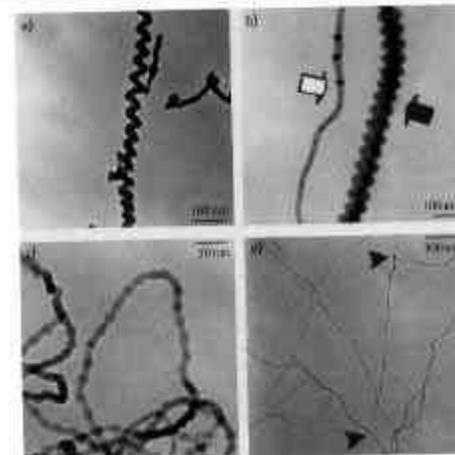


Fig. 4.10a-d TEM images of four special forms of Si nanowires synthesized by the laser ablation of a Si powder target. (a) A spring-shaped Si nanowire; (b) fishbone-shaped (indicated by a solid arrow) and frog-egg-shaped (indicated by a hollow arrow) Si nanowires; and (c) pearl-shaped nanowires, while (d) shows a poly sites for the nucleation of silicon nanowires (indicated by arrows) [4.116]

Nanostrutture di carbonio (e silicio?)

Natura dei legami tra atomi di carbonio dà origine ad ampia varietà di angoli di legame C-C → **clusters di carbonio (fullereni)**

Table 5.1. Types of sp^n hybridization, the resulting bond angles, and examples of molecules

Type of Hybridization	Digonal sp	Trigonal sp^2	Tetrahedral sp^3
Orbitals used for bond	s, p_z	s, p_x, p_y	s, p_x, p_y, p_z
Example	Acetylene C_2H_2	Ethylene C_2H_4	Methane CH_4
Value of λ	1	$2^{1/2}$	$3^{1/2}$
Bond angle	180°	120°	$109^\circ 28'$

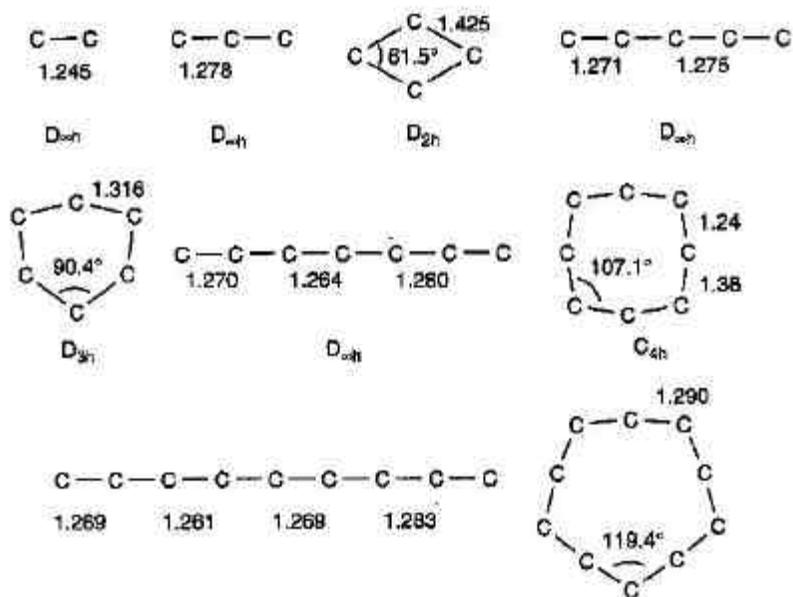
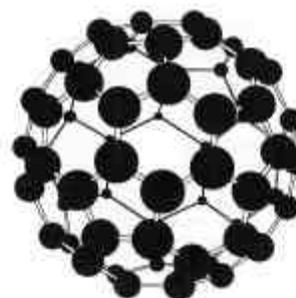
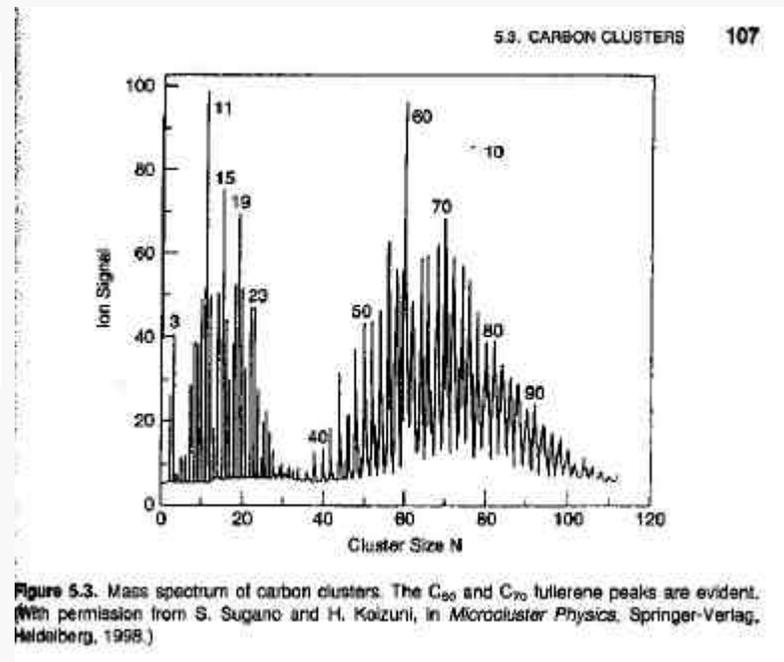


Figure 5.4. Some examples of the structures of small carbon clusters. [With permission from Raghavacari et al., *J. Chem. Phys.* **87**, 2191 (1987).]



atom it becomes electrically conducting. Figure 5.7 shows the location of the alkali atoms in the lattice where they occupy the two vacant tetrahedral sites and a larger octahedral site per C₆₀ molecule. In the tetrahedral site the alkali atom has four surrounding C₆₀ balls, and in the octahedral site there are six surrounding C₆₀

Numeri magici e
strutture ad alta
simmetria

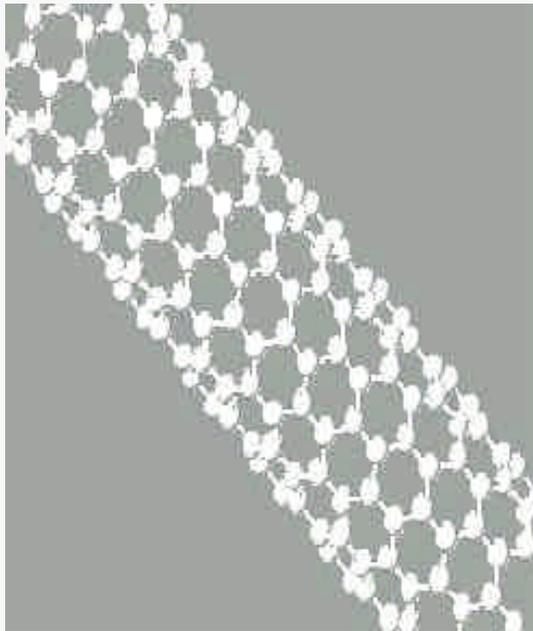
Nanotubi di carbonio (CNT)*

Anni 80: osservazione di molecole di fullerene (C_{60} , ...)

Inizio anni 90: produzione in laboratorio di fullerene (Nobel 96)

Fine anni 90: produzione di nanotubi di carbonio con forti **motivazioni nanotecnologiche**

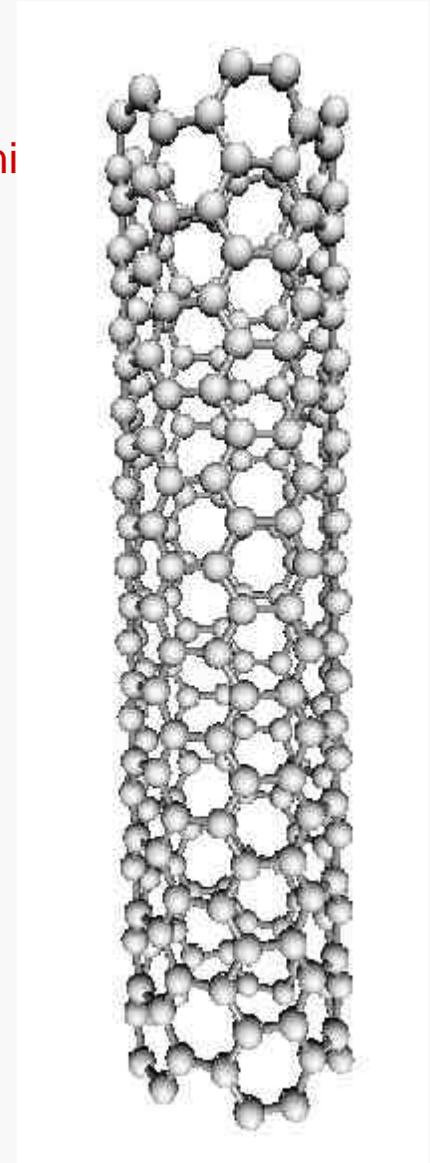
Nanotubi: fogli di grafite (graphene - struttura esagonale) ripiegati a formare **cilindri cavi**



Single Wall NT

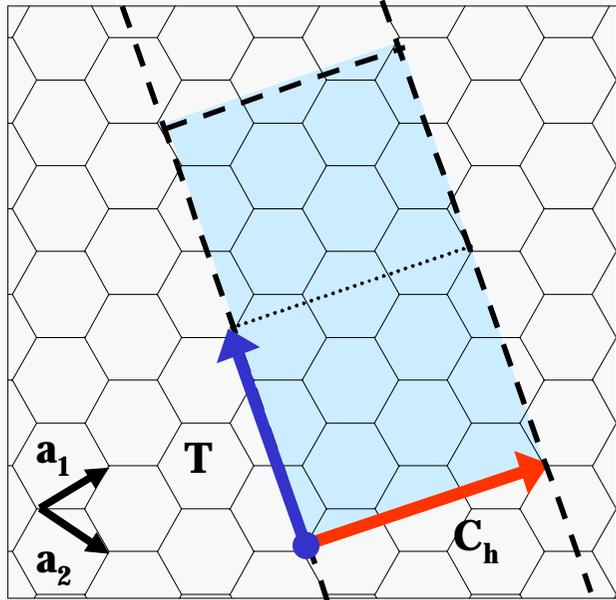


Multiple Wall NT



* Materiale sui CNT tratto in parte da un seminario di Andrea Ferrari, EDM - Cambridge University (lug. 2002)

Classificazione CNT



Strutture 1D con legami sp^2

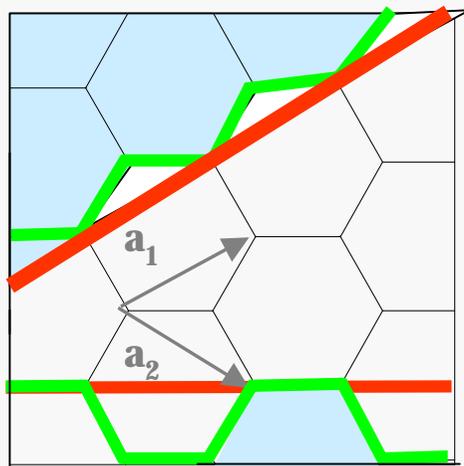
Cella unitaria descritta da:

– chiral vector

$$\mathbf{C}_h = n\mathbf{a}_1 + m\mathbf{a}_2 \quad \forall n, m \in \mathbb{Z}$$

– translation vector

$$\mathbf{T} = t_1\mathbf{a}_1 + t_2\mathbf{a}_2 \quad \forall t_1, t_2 \in \mathbb{Z}$$



Zigzag $(n, 0)$ tube
 $\mathbf{C}_h \parallel \mathbf{a}_1$ (or \mathbf{a}_2)

Armchair (n, n) tube

[Chiral (n, m) tube]

Proprietà geometriche CNT
 completamente determinate da
 vettore chirale e di traslazione (cioè
 da numeri (n, m))

$$\text{Diametro NT: } d_{NT} \propto \sqrt{(m^2 + n^2 + nm)}$$

Distanza tra primi vicini $\sim 1.42 \text{ \AA}$

Proprietà elettroniche CNT I

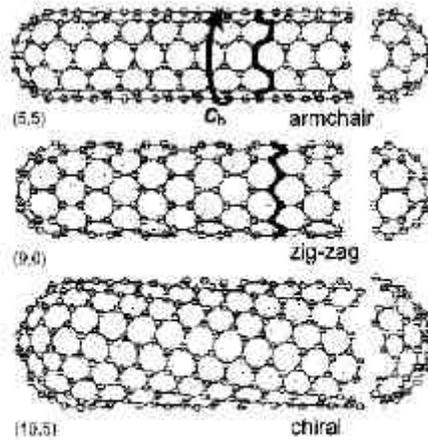


Figure 4: Examples of CNTs with different circumference vectors C_n [5]

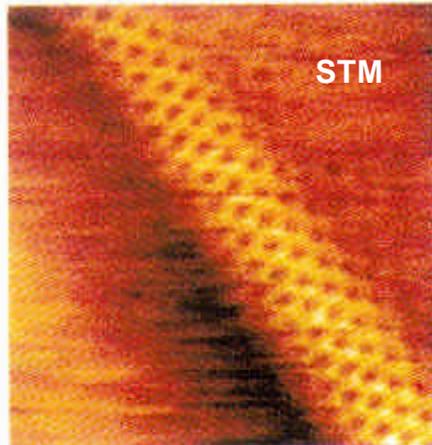


Figure 5: STM image at 77 K of a SWNT at the surface of a rope [6]

Da R. Waser Ed., Nanoelectronics and information technology (Wiley-VCH, 2003)

2.1 Geometrical Structure

The structure of CNTs is described by the circumference vector or **chiral vector** C_n , which represents the full circumference of the tube. It is defined by

$$C_n = n\mathbf{a}_1 + m\mathbf{a}_2 \quad (1)$$

where \mathbf{a}_1 and \mathbf{a}_2 are the unit vectors in the hexagonal lattice, and n and m are integers (Figure 1). C_n also defines the propagation vector P_n , representing the periodicity of the tube parallel to the tube axis. Furthermore, it settles the so-called chiral angle which is the angle between C_n and \mathbf{a}_1 . If either n or m are zero, the chiral angle is 0° and the structure is called *zig-zag*. If $n = m$, the chiral angle is 30° and the structure is called *armchair* (Figure 4). All other nanotubes show chiral angles between 0° and 30° . They are known as *chiral* nanotubes because they produce a mirror image of their structure upon an exchange of n and m .

Experimentally, the diameter of nanotubes is frequently determined by TEM, STM or AFM. The chiral structure can be determined by STM (Figure 5).

2.2 Electronic Structure of Graphene

For the discussion of the electronic structure of CNTs, we start again with graphene. As an extension of the description of fused benzene (Chap. 5), in graphene, a bonding π -band and an anti-bonding π^* -band is formed from the overlap between $2p_z$ -AOs of adjacent atoms. P. R. Wallace [7] derived an expression for the 2-D energy states, W_{2D} , of the π -electrons in the graphene plane as a function of the wave vectors k_x and k_y (see also [8]):

$$W_{2D}(k_x, k_y) = \pm \gamma_0 \left[1 + 4 \cos\left(\frac{\sqrt{3}k_x a}{2}\right) \cos\left(\frac{k_y a}{2}\right) + 4 \cos^2\left(\frac{k_y a}{2}\right) \right]^{1/2} \quad (2)$$

where γ_0 denotes the nearest-neighbour overlap (or: transfer) integral and $a = 0.246$ nm is the in-plane lattice constant. The two different signs in Eq. (2) represent the π - and π^* -band. The calculations show that the π - and π^* -band just touch each other at the corners of the 2-D Brillouin zone (Figure 6). In the vicinity of the Γ point, the dispersion relation is parabolically shaped, while towards the corners (K points) it shows a linear $W(k)$ dependence. At $T = 0$ K, the π -band is completely filled with electrons and the π^* -band is empty. Because the bands only touch at the K points, integration over the Fermi surface (which is a line for a two-dimensional system) results in a vanishing density of states. On the other hand no energy gap exists in the graphene dispersion relation. This means we are dealing with the unusual situation of a **gapless semiconductor**. (The real graphite yet is a metal since the bands overlap by approx. 40 meV due to the interaction of the graphene planes.)

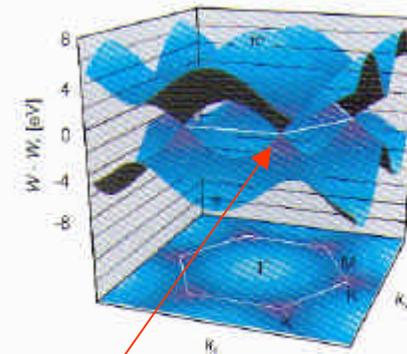


Figure 6: 3-D illustration of the dispersion relation of graphene.

Graphene:
"semiconduttore a gap nullo"

Proprietà elettroniche CNT II

2.3 Electronic Structure of Carbon Nanotubes

For the description of the band structure of graphene, it has been assumed that the graphene plane is infinite in two dimensions. For CNTs, we have a structure which is macroscopic along the tube axis, but the circumference is in atomic dimensions. Hence, with the density of allowed quantum mechanical states in axial direction will be high, the number of states in the circumferential direction will be very limited. More precisely, the roll-up by the chiral vector C_h leads to periodic boundary conditions in the circumferential direction. Quantum mechanically, these boundary conditions define allowed modes (1-D states) along the tube axis according to:

$$C_h \cdot k = 2\pi j \quad \text{with } |j| = 0, 1, 2, \dots$$

In the case of arm-chair tubes, the periodic boundary condition yield allowed values for the wave vector in circumferential direction according to:

$$k_{x,j} = \frac{j}{q_y} \frac{2\pi}{\sqrt{3}a}$$

where $q_y = n - m$. For the armchair geometry, the tube axis is identical to the x -direction and the circumference represents the y -direction. As an example of an armchair tube, Figure 7 shows the dispersion relation, the projection of the allowed 1-D states onto the first Brillouin zone of graphene, as well as the $W(k_x)$ relation for a (3,3) tube. Due to the periodic boundary conditions, i. e. by inserting Eq. (4) into Eq. (2), the allowed states condense into lines (black lines in Figure 7a). Here, there are $q_y = 3$ lines on either side of the center of the Brillouin zone and an additional line going through the center. In case of a (3,3) tube the allowed states include the K points. Since the system is now one-dimensional in an electronic sense, different from the case of graphene, the integration over the Fermi surface (which is the sum over the Fermi points) yields a finite density of states at the Fermi energy. The (3,3) tube, and armchair tubes in general, show a metallic behavior.

As an example of a chiral tube, Figure 8 shows the dispersion relation, the projection of the allowed 1-D states onto the first Brillouin zone of graphene, as well as the $W(k_x)$ relation for a (4,2) tube. We will illustrate why the electronic properties of this (4,2) tube is very different from the (3,3) tube despite their very similar diameters. Again, due to the periodic boundary conditions, the allowed states condense into lines (black lines in Figure 8a). In contrast to the (3,3) tube, the C_h vector is not parallel to the y -direction and, hence, leads to a mixed quantization of k_x and k_y . The propagation of an electron along the tube axis is described by a combination of k_x and k_y -components. For this reason, the general letter k is used in Figure 8c, representing the momentum of the electron in the direction of propagation. The band structure of (4,2) tubes is deter-

DOS e geometria CNT

Armchair CNT

mined by the fact that there are no modes which include the K points of the Brillouin zone of graphene (Figure 8b). The Fermi level is not dependent on the C_h vector, W_F is now in a bandgap, i. e. this type of tube is a semiconductor. The bandgap is of the order of a few eV (Figure 8c). In general, the bandgap decreases with increasing diameter of the tube.

In general, the semiconducting or metallic behavior of CNTs is controlled by the C_h vector and, hence, by the relation of n and m . Metallic behavior occurs for

$$n - m = 3q \quad (5)$$

where q is an integer. As a consequence, one-third of all CNTs types are metallic for a statistic distribution of chiralities including all armchair types, since $q = 0$ for them.

The periodic boundary conditions for zig-zag tubes, $(n,0)$ tubes and $(0,m)$ tubes, results in allowed wave vectors according to

$$k_{x,j} = \frac{j}{q_x} \frac{2\pi}{a} \quad (6)$$

The condition for metallic tubes, Eq. (5), is fulfilled for one-third of the tubes, i. e. if n or m are multiples of three. Figure 9 illustrates the density of state (DOS) for two zig-zag type CNTs [9], a (10,0) tube showing a bandgap and, hence, semiconducting behavior (Figure 9a), and a (9,0) tube showing no bandgap and, hence, metallic behavior (Figure 9b).

The discussion so far has been restricted to isolated SWNTs. Theoretical and experimental studies have shown that the intertube coupling within MWNTs and ropes of SWNTs [10], [11] have a relatively small effect on the band structure of a tube [12]. As a consequence, semiconducting and metallic tubes retain their character if they are a part of MWNTs or ropes. By statistical probability, most of the MWNTs and ropes show an overall metallic behavior, because one single metallic tube is sufficient to short-circuit all semiconducting tubes.

Chiral CNT

Metal/semi

SWNT/MWNT

Proprietà elettroniche dipendenti da struttura:

- Metalli per armchair (n, n)
- Semimetalli per $n - m = 3i$ (i intero)
- Semicond. altrimenti

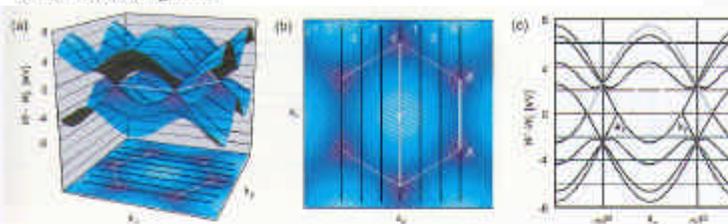
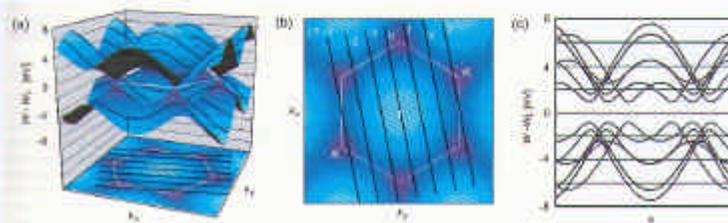
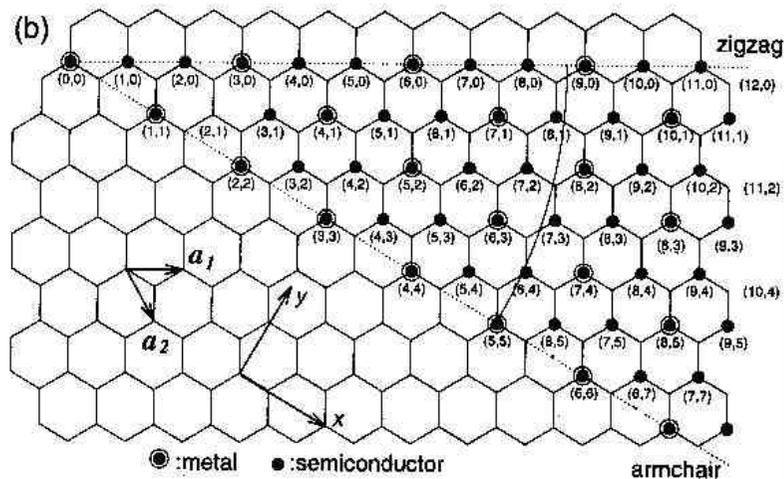
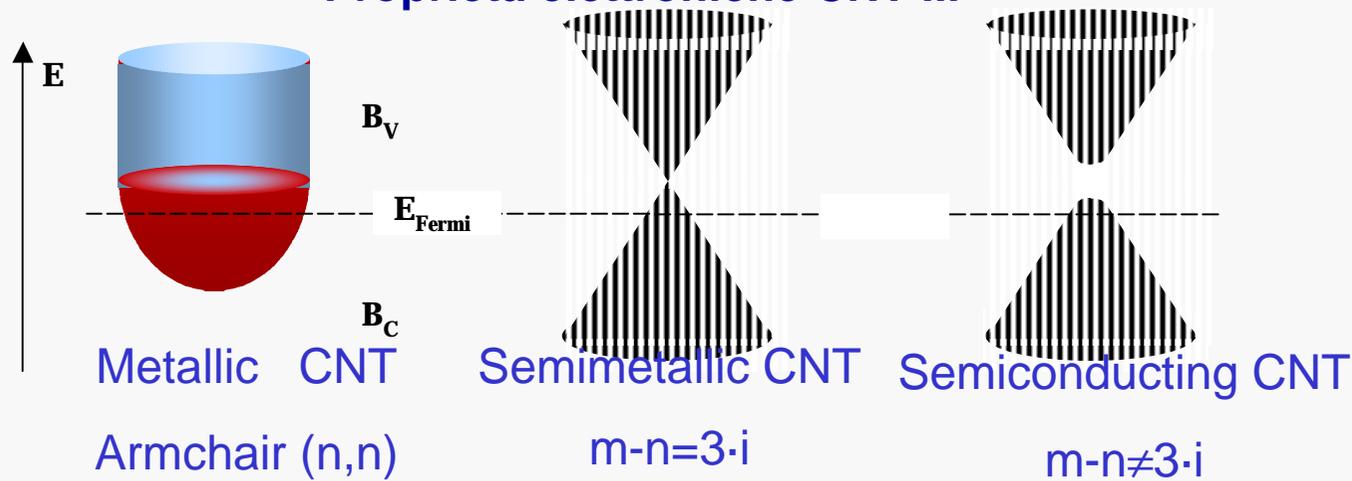


Figure 7 Dispersion relation of a (3,3) CNT. (a) 3-D illustration of the dispersion relation for graphene including the allowed states for the (3,3) CNT. The periodic boundary conditions along the circumference of the tube result in discrete wave vectors k_x values. (b) Projection of the allowed states onto the first Brillouin zone of graphene (observe the K points are allowed states for CNTs of this chirality). (c) 2-D illustration of the dispersion $W(k_x)$. The states at the Fermi level indicate the metallic behavior of this tube. The periodicity visible in the legend is given by the interval $\Delta k_x = \pi/a \sqrt{3}$.

Figure 8 Dispersion relation of a (4,2) CNT. (a) 3-D illustration of the dispersion relation for graphene including the allowed states for the (4,2) CNT. The periodic boundary conditions along the circumference of the tube result in a discrete set of allowed k_x values. (b) Projection of the allowed states onto the first Brillouin zone of graphene (observe the K points are not allowed states for CNTs of this chirality). (c) 2-D illustration of the dispersion $W(k)$. The conduction band and the valence band are separated by a bandgap.



Proprietà elettroniche CNT III



Altre proprietà fisiche di grande rilievo

- Mechanical properties
 - High elastic modulus (up to 1TPa)
 - Tensile strength (45GPa)
- Thermal properties
 - High thermal conductivity (~6600 W/m K)
 - High thermal stability
- Large surface area

Tuneable band gap ($2 \cdot 10^{-3}$ -1.1eV)

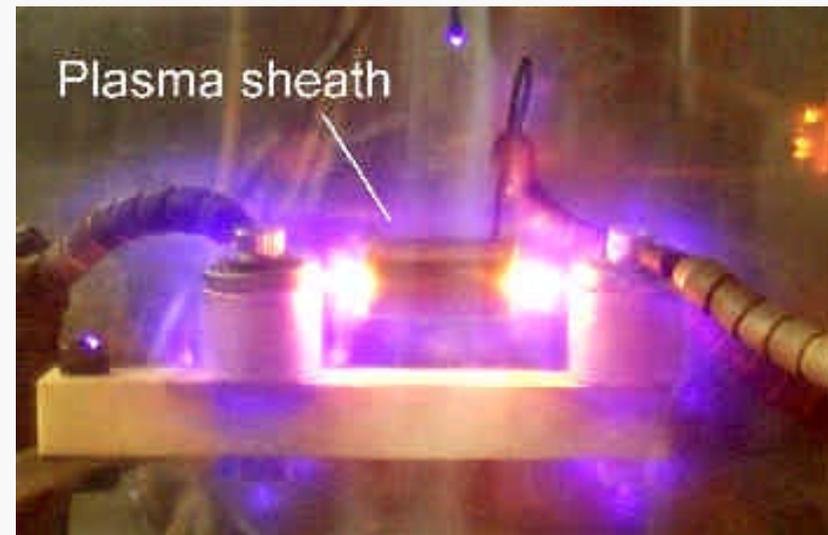
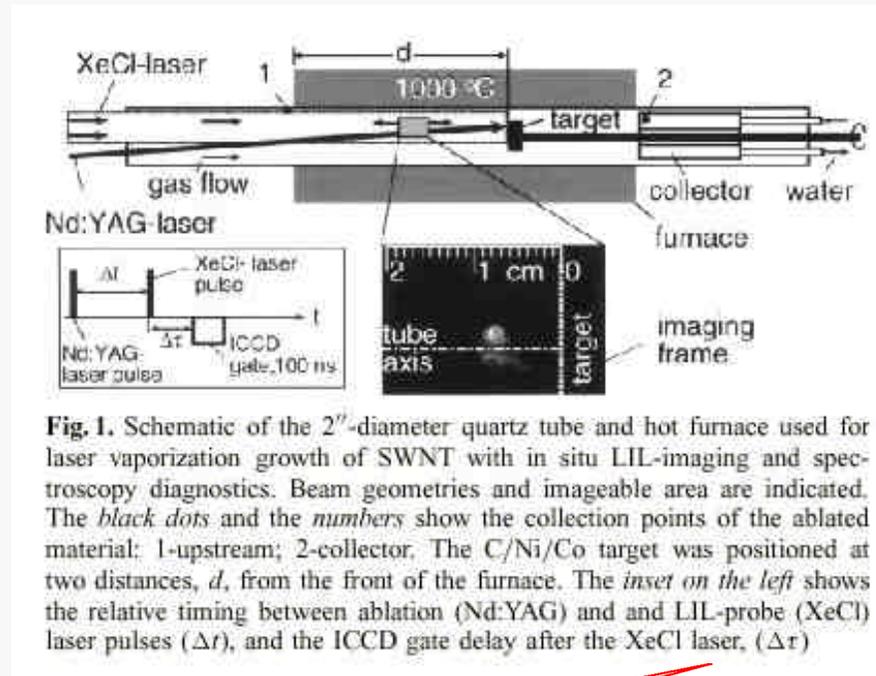
- $E_g \sim 1/d_{NT}$ also affected by:
 chemical doping (B, N, O, Li, K...)
 point defects (pentagons, heptagons)

Fabbricazione di CNT

CNT richiedono processo di fabbricazione “violento” (alte T, P, quantità di materiale)

Metodi di deposizione più comuni:

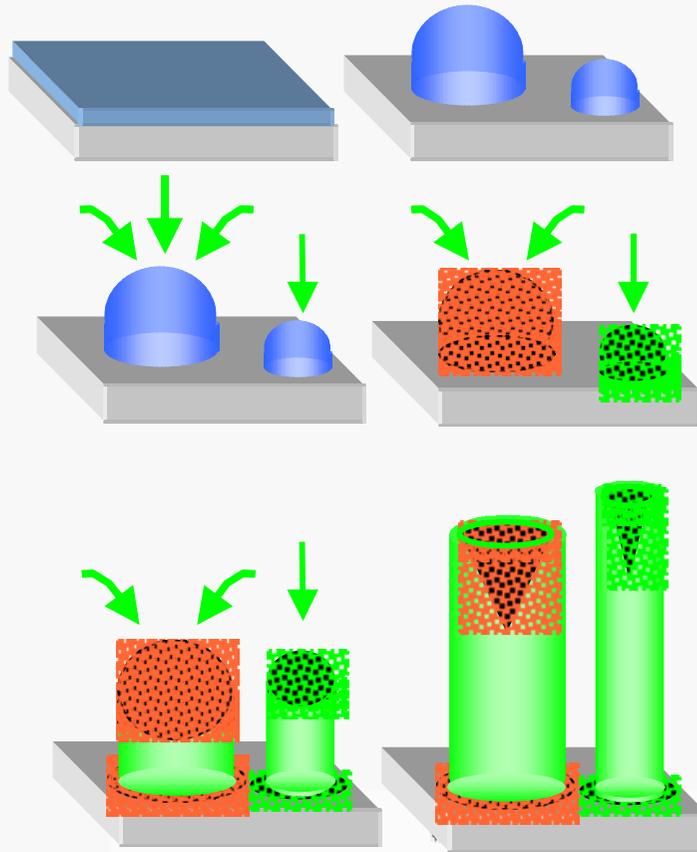
- Laser Ablation (spesso “alla Smalley”) --> SWCNT con diametro controllato
- Scarica ad arco (come fullereni) --> grandi quantità, scarso controllo
- PE-CVD da C_xH_x --> grande efficienza soprattutto per MWCNT



- Up to 900°C heated stage
- C_2H_2/NH_3 up to 200sccm

See Puretzky, Geohegan,...
Appl. Phys. A 70 153 (2000)

Ruolo catalizzatori metallici



- During annealing/etching the metal layer dewets the substrate forming droplets
- Carbon dissolves into the catalyst material and forms a solid solution
- After saturation, carbon precipitates starting the NT growth
- The metal droplet is lifted at the growing edge

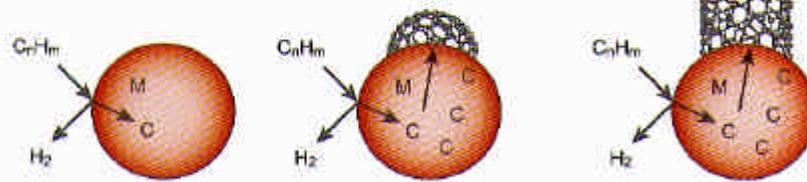


Figure 16: Root-growth mechanism for the formation of a single-wall carbon nanotube from a metal nanoparticle, by chemical vapor deposition:

(a) decomposition of the hydrocarbon on the nanoparticle and solubilization of the carbon therein.

(b) nucleation by formation of a fullerene cap.

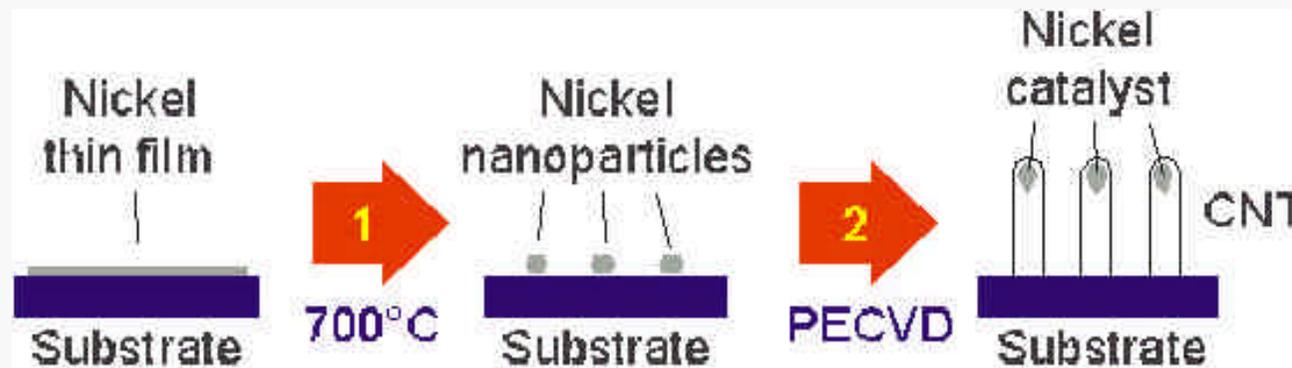
(c) elongation of the SWNT by incorporation of further carbon into the metal-carbon bonds at the growing end.

Esempi di catalizzatori nanostrutturati

Processo di crescita catalitico (Ni or Co nanoparticles)



necessità produzione nanoparticles

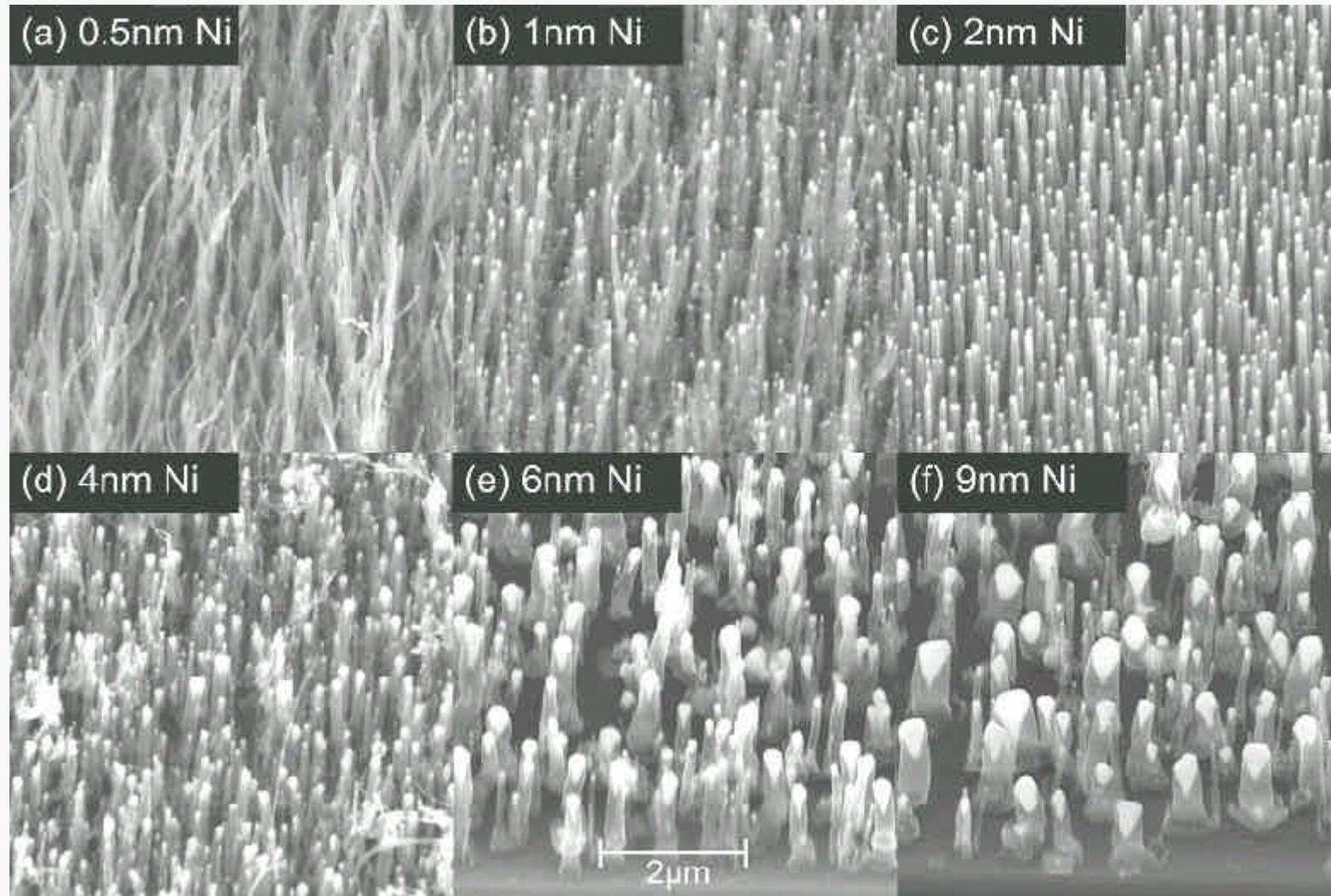


- **Step 1:** At 700°C (growth temp), Ni film sinters into catalyst nanoparticles.
- **Step 2:** PECVD - C₂H₂ is the growth gas for CNTs, NH₃ is the etching gas for unwanted a-C.

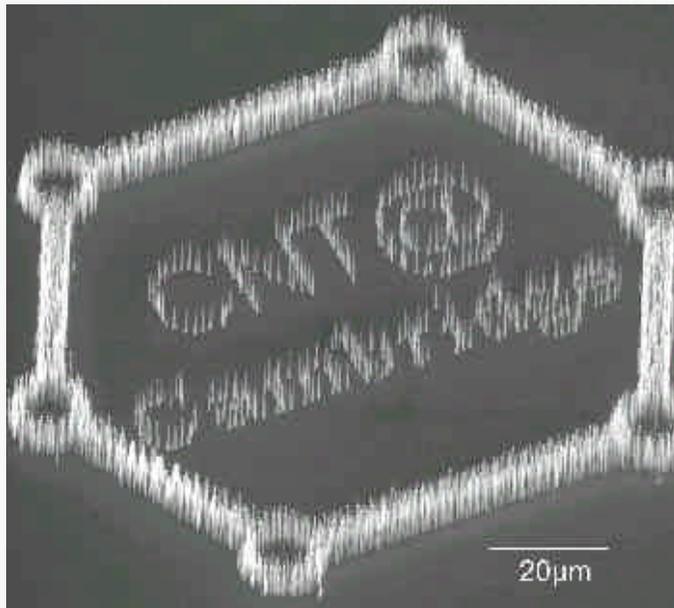
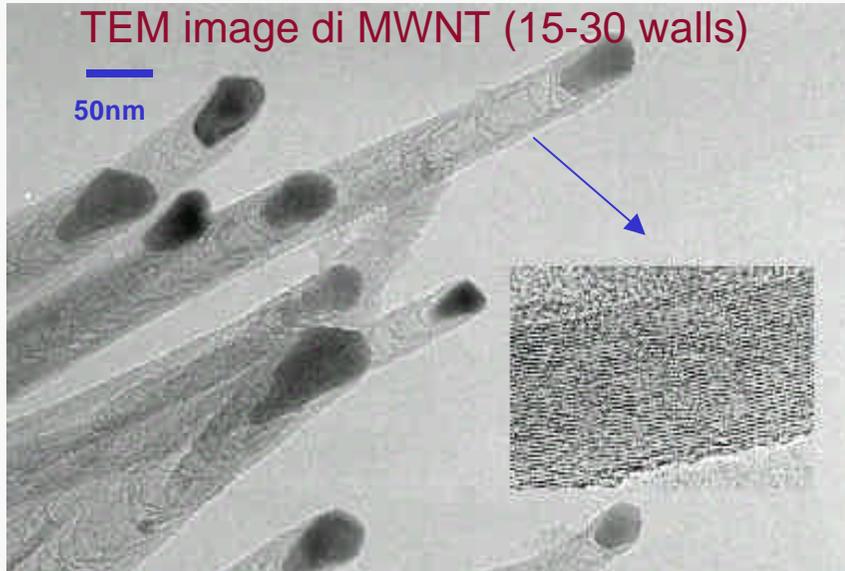
Catalizzatori “determinano” ancoraggio CNT su substrato

Strutturazione catalizzatori → strutturazione CNT

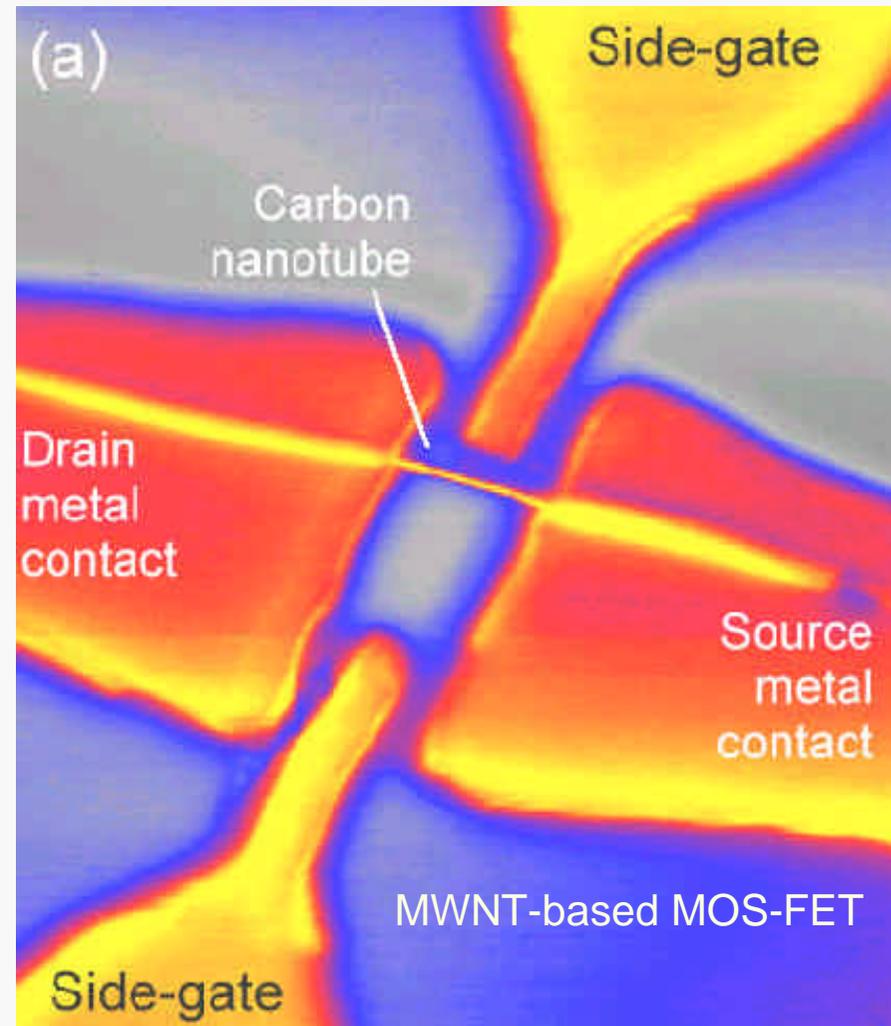
Influenza catalizzatore (diametro Ni nanoparticles)



Esempi CNT



Litografia nanoparticles --> strutture di CNT



Esempi di applicazioni elettroniche per CNT

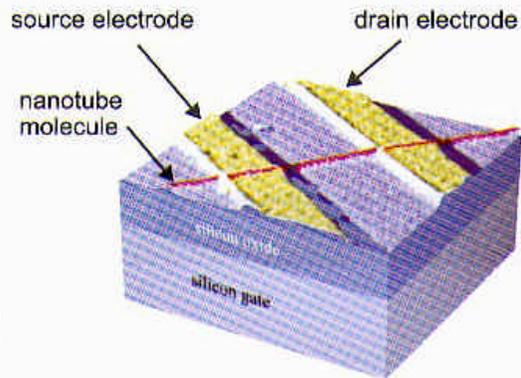


Figure 25: A carbon nanotube field-effect transistor (CNTFE) nanotube (red) is located between two platinum contacts (yellow). The back-gate-stack (blue) is formed by a silicon dioxide dielectric on top of a silicon wafer (colored AFM-image taken from [57]).

MOS-FET

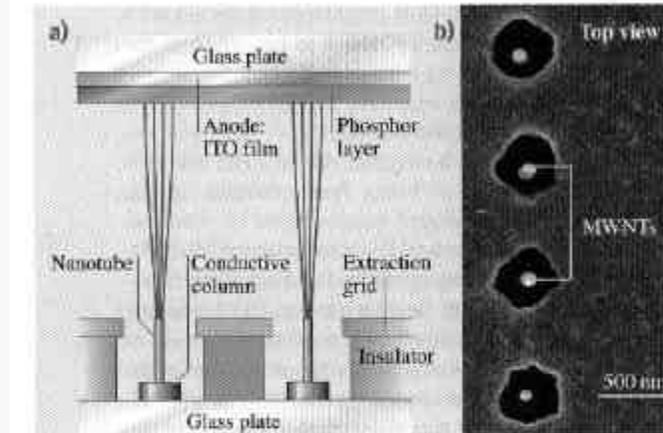


Fig. 3.28 (a) Principle of a field-emitter-based screen. (b) Scanning electron microscope image of a nanotube-based emitter system (top view). Round dots are MWNT tips seen through the holes corresponding to the extraction grid. By courtesy of Legayneux (Thales Research & Technology, Orsay, USA)

Field-emitter

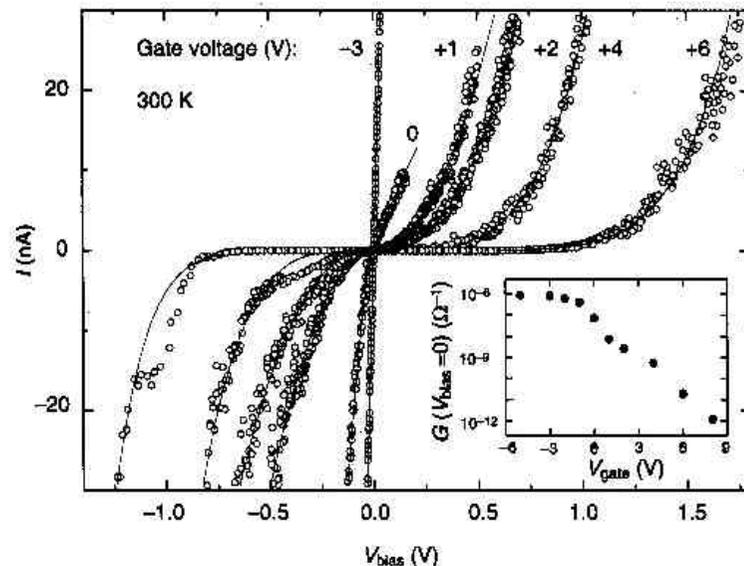
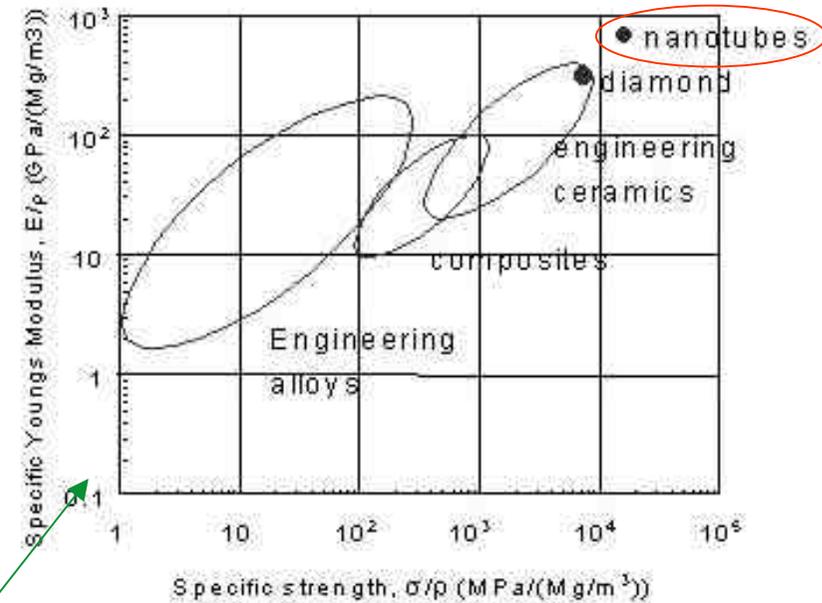


Figure 26: The current-voltage characteristics of a semiconducting single-wall carbon nanotube for different gate voltages (see Figure 25). For large positive gate voltages the conductance of the tube is very small for source-drain biases less than approximately 1 V. Changing the gate voltage to negative values increases the conductivity steadily until saturation is reached at approximately -3 V (see insert). The maximum conductivity is comparable to the values found for metallic tubes measured in the same experiment (taken from [57]).

Alcune applicazioni possibili per CNT

- Hydrogen and ion (Li) storage units
- Supercapacitors, fuel cells, batteries
- Gas sensors
- **FE devices (field emitters)**
- **Advanced scanning probes (SEM)**
- **Superstrong and tough composites (nanocomposites)**
- Templates for metal nanowires
- **Actuators (NanoElectroMechanical Systems - NEMS)**
- ...



Comparison of Specific Young's Modulus vs. Specific Strength for nanotubes and other engineering materials

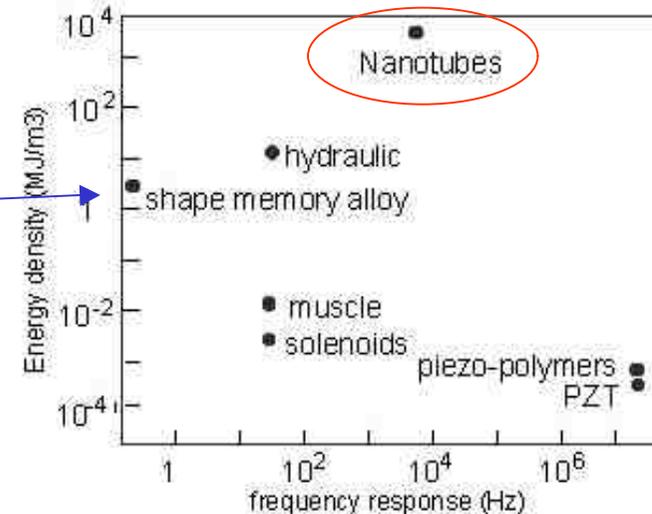
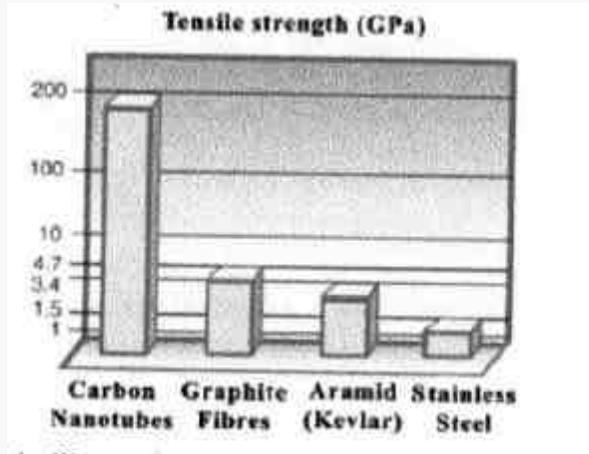


Fig. 3. Energy Density vs. Frequency response of Actuator materials

Proprietà meccaniche di CNT

Eccezionale modulo elastico



Moduli di Young, di taglio, e di bulk simili a diamante

Grande resistenza allo sforzo dovuta a forza dei legami inter-carbonio e geometria dei CNT

Materiale tratto dal seminario di Francesco Greco, febbraio 2003

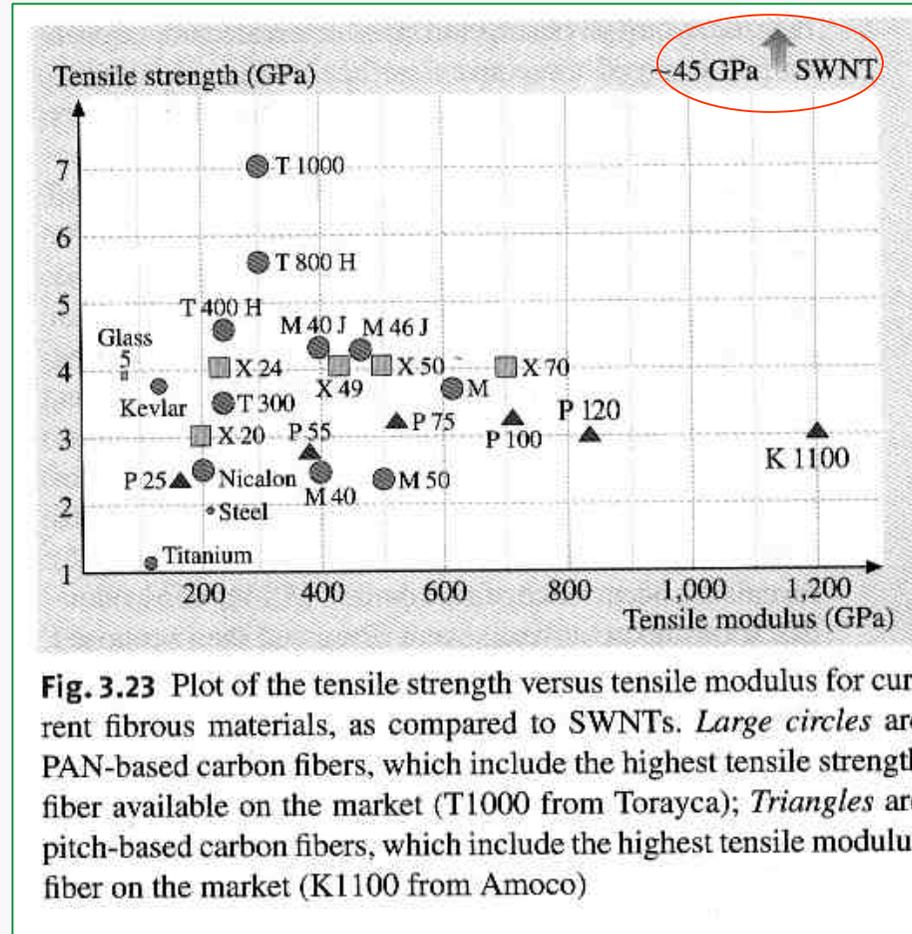


Fig. 3.23 Plot of the tensile strength versus tensile modulus for current fibrous materials, as compared to SWNTs. Large circles are PAN-based carbon fibers, which include the highest tensile strength fiber available on the market (T1000 from Torayca); Triangles are pitch-based carbon fibers, which include the highest tensile modulus fiber on the market (K1100 from Amoco)

Elasticità eccellente rispetto a fibre di carbonio (compositi) ordinarie

Duttilità/fragilità di CNT

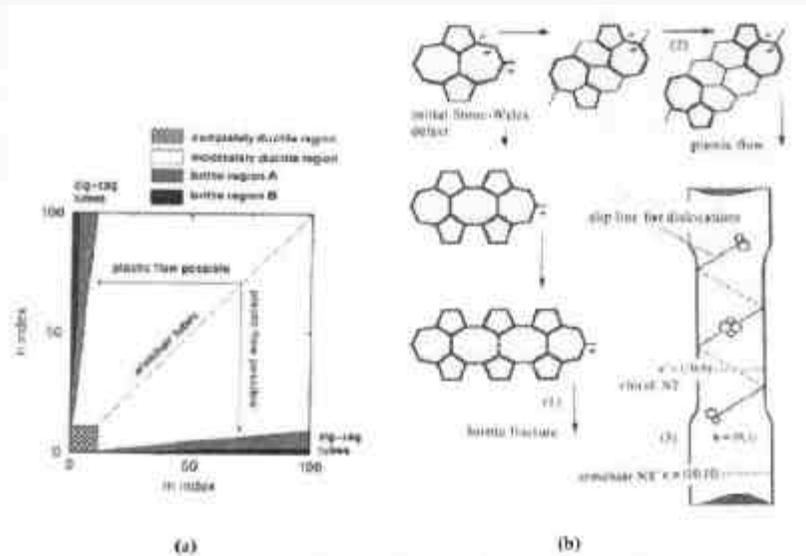
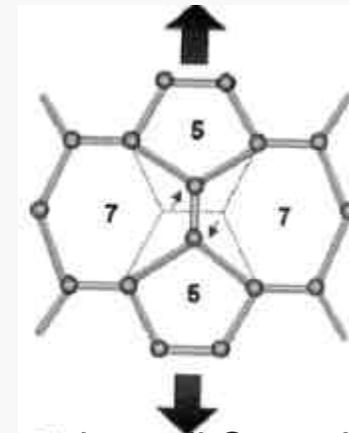


Figura 23 – (a) Mappa dei domini duttile/fragile per nanotubi di carbonio con diametri fino a 13 nm. Aree con diversa ombreggiatura corrispondono a differenti comportamenti del materiale; (b) Processo di propagazione di difetti in un nanotubo armchair con un iniziale difetto Stone-Wales. (1) frattura; (2) una coppia di dislocazioni scivolano via l'una dall'altra; (3) il cambio di chiralità del nanotubo e il graduale cambiamento del diametro causano una corrispondente variazione nelle proprietà elettriche. La formazione di ulteriori difetti Stone-Wales continua il processo di restringimento a meno che le dislocazioni non si impilino a causa della bassa temperatura che limita la mobilità sui tubi.



Deformazione di Stone Wales

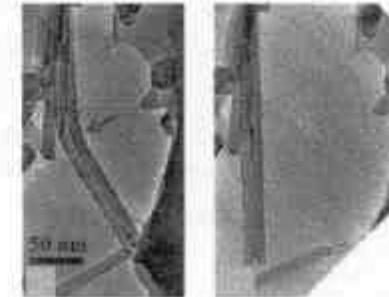


Figura 27 – Due immagini TEM mostrano un nanotubo (sx) originariamente piegato a temperatura ambiente e (dx.) dopo il riscaldamento

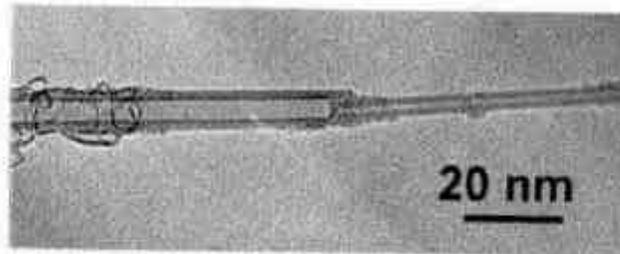


Figura 21 - Immagine TEM. Il nucleo interno a 4 strati è stato estratto (comportamento telescopico).

Esempio di sfilamento per stiro dei nanotubi interni (in MWNT) sotto sforzo di rottura

Recupero di forma tramite riscaldamento

Studio nanoscopico proprietà meccaniche

Studio mediante AFM dello stress/strain di MWCNT

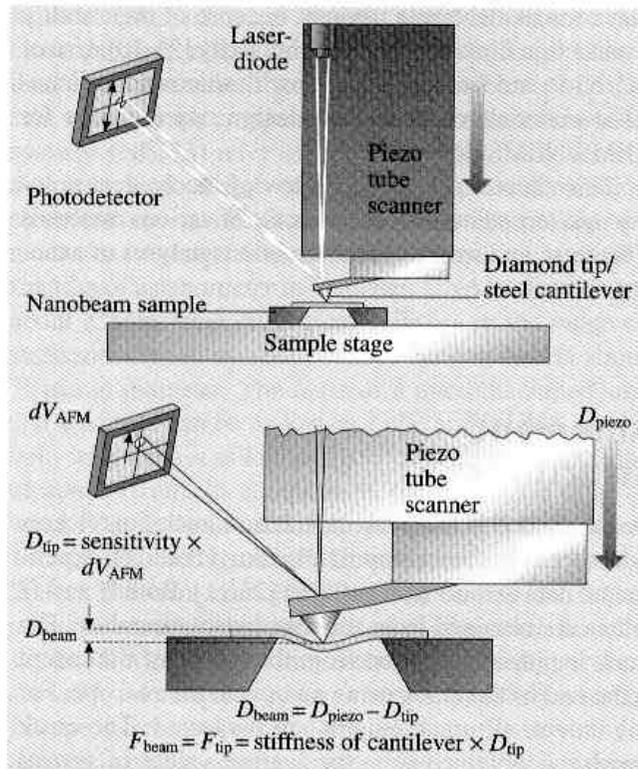
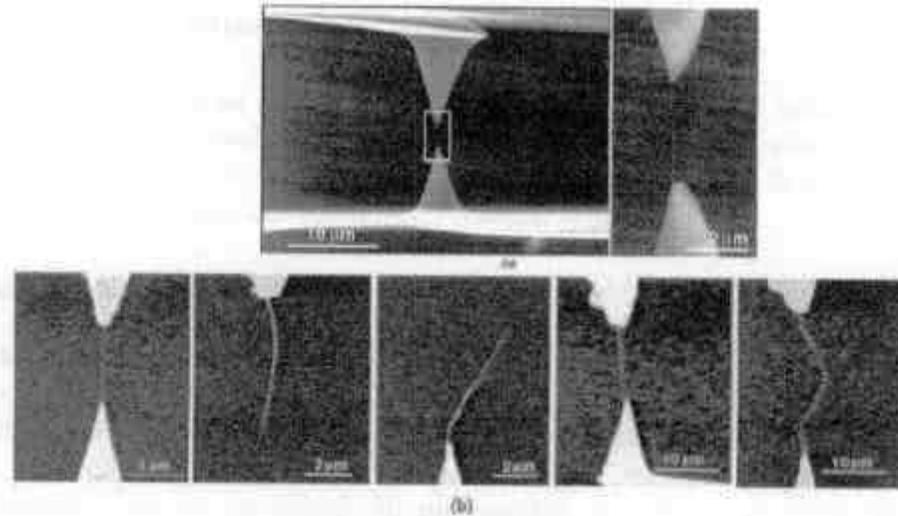


Fig. 25.1 Schematic showing the details of a nanoscale bending test. The AFM tip is brought to the center of the nanobeam and the piezo is extended over a known distance. By measuring the tip displacement, a load-displacement curve of the nanobeam can be obtained [25.38]

“Nanodeformazioni”
applicate tramite AFM



- Immagini SEM che mostrano (a) l'apparato per la misura di carico tensile di MWCNT con un taccato a due punte AFM opposte prima dell'imposizione del carico; (b) il meccanismo di frattura "telescopico" tipico dei MWCNTs.

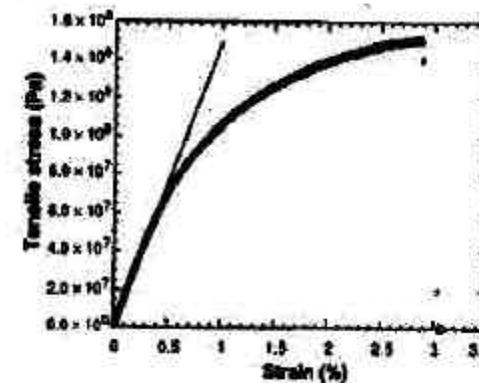


Figura 20 - Grafico stress-strain in misure tensili condotte su fibre di SWCNT.

Nanotubi in materiali multi-funzionali

Table 3.5 Applications for nanotube-based multifunctional materials (from [3.3]), by courtesy of B. Maruyama (WPAFB, Dayton, Ohio)

Fiber fraction	Applications system	Mechanical			Electrical			Thermal		Thermo-mechanical	
		Strength/stiffness	Specific strength	through-thickness strength	Static dissipation	Surface Conduction ^a	EMI shielding	Service ^b temp.	conduction/dissipation ^c	Dimensional Stability ^d	CTE reduction ^e
Low Volume fraction (fillers)											
Elastomers	Tires	x			x					x	
Thermo Plastics	Chip package Electronics/Housing	x			x		x	x	x		
Thermosets	Epoxy products Composites	x	x	x		x				x	x
High Volume Fraction											
Structural composites	Space/aircraft components		x	x							
High conduction composites	Radiators Heat exchangers EMI shield	x						x	x	x	x

^a For electrostatic painting, to mitigate lightning strikes on aircraft, etc.

^b To increase service temperature rating of product

^c To reduce operating temperatures of electronic packages

^d Reduces warping

^e Reduces microcracking damage in composites

Applicazioni meccaniche di nanocompositi con nanotubi in diversi settori

Nanocompositi a base di CNT

CNT rinforzano matrici polimeriche, ma occorre alta compatibilità per evitare sfilamento nanotubi

CNT/polivinilalcol

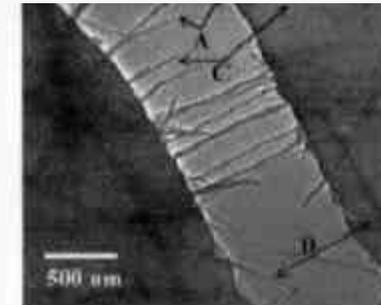


Figura 26 – Immagine SEM della superficie si frattura in un composito a base di nanotubi di carbonio.

Esempi di funzionalizzazione

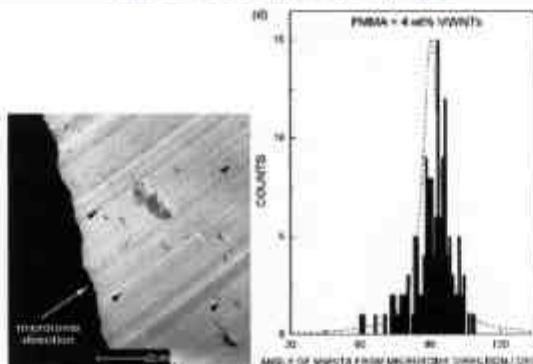
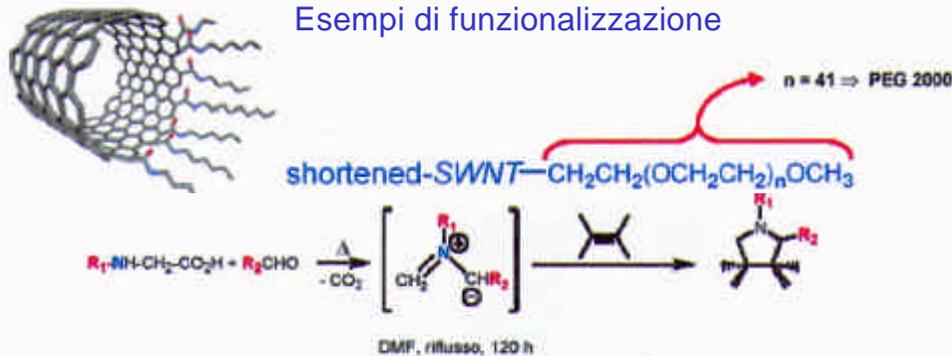


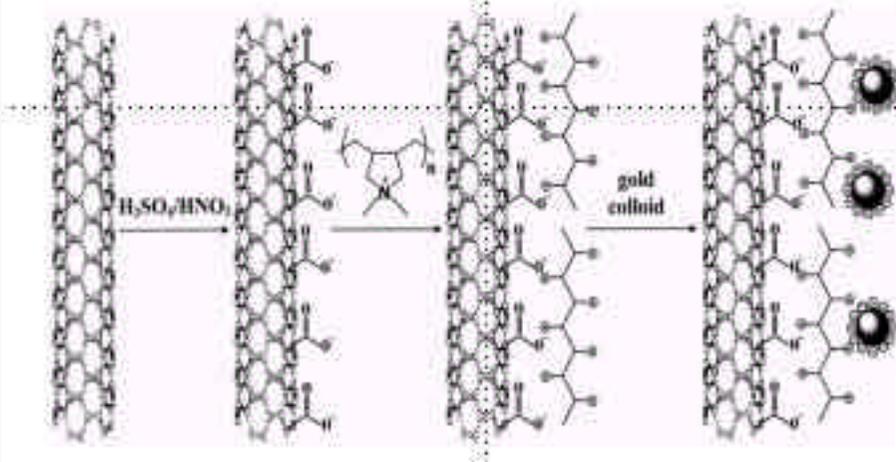
Figura 32 – (ix) Immagine TEM di un composito MWNT (4% in peso) in una matrice di PMMA. La freccia bianca indica la direzione del taglio (90° rispetto alla direzione di estrusione). Le frecce nere indicano i nanotubi. (ix) Istogramma che riporta la distribuzione di orientazione di MWCNT nel composito. La linea tratteggiata corrisponde a un fitting Lorentziano dei dati.

CNT funzionalizzato per solubilizzarlo in matrici polimeriche (es.: polietilenglicole attaccato a estremità di CNT “spezzati”, oppure AIBN - azobisisobutirronitrile che inizia legami covalenti tra carbonio e PMMA) oppure surfattanti non-ionici per aumentare wettability oppure miscelamenti meccanici prolungati (Brabender a doppia vite e temperatura alta)

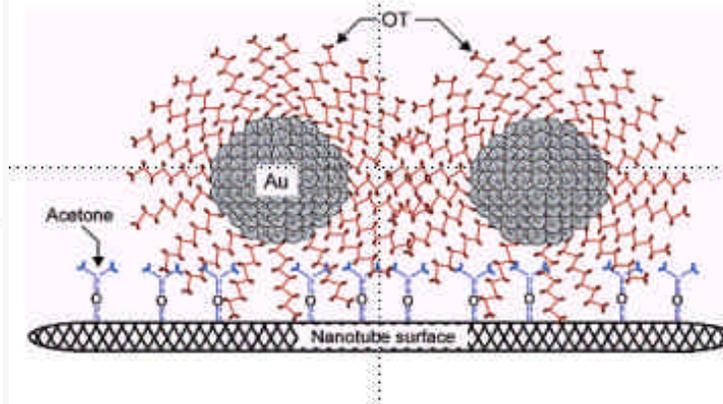
Incremento modulo elastico 10 volte più efficiente che con ordinarie fibre di carbonio (a pari peso)

Altri esempi di funzionalizzazione di CNT

Una prima reazione prevede la sospensione dei nanotubi in una soluzione 3:1 di acido solforico e nitrico in un bagno sonico per due ore, quindi per reazione con PDADMAC (polidialildimetilammonio-Cloruro) che si aggancia ai gruppi carbossilici presenti in superficie, le particelle d'oro con diametro di 10 nm possono aderire:



Schematizzazione dell'attacco dei cluster di oro sulla superficie dei nanotubi:



ANCORAGGIO DI NANOCLUSTER D'ORO SULLA SUPERFICIE DI NANOTUBI DI CARBONIO MODIFICATI

La modifica con acetone della superficie dei nanotubi di carbonio permette l'adesione di cluster metallici.

Nanoparticelle d'oro stabilizzate da opportuni leganti come tioli (o ammine) possono essere dunque adese su tali superfici dando luogo a strutture che potranno essere impiegate in nanodispositivi ibridi bio-inspired.

Infatti c'è un grande studio sulla possibilità di far aderire opportuni cluster stabilizzati da proteine su questi nanotubi quali parte di nanodispositivi.

Per quanto riguarda il meccanismo di attacco esso è stato ipotizzato dai valori degli stretching asimmetrici dei CH_2 e CH_3 prima e dopo l'attacco dei cluster sui nanotubi e la conclusione è che si tratti di un'interazione tra le catene alchiliche dell'OT (ottandiolo) con i gruppi metilici dell'acetone.

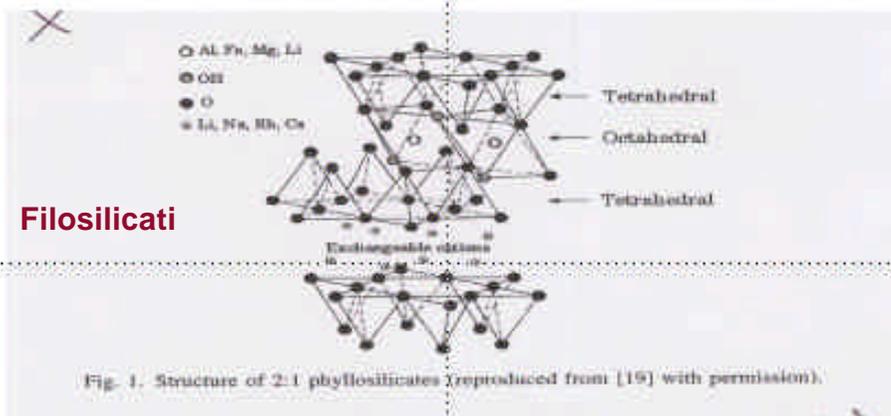
Esempi di funzionalizzazione con nanoparticelle d'oro

Interesse per la realizzazione di possibili dispositivi biocompatibili

Materiale tratto dal seminario di
M. Barnabò, Aprile 2004

Cenni su nanocompositi polimerici I

I silicati comunemente usati per i nanocompositi appartengono, come struttura, alla famiglia dei 2:1 fillosilicati



La struttura consiste di un strato bi-dimensionale con al centro un ottaedro di alluminio o magnesio legati tramite gruppi OH a tetraedri di silicio superiori e inferiori. Ha uno spessore di circa un 1 nm e le dimensioni laterali variano da 300 Å a qualche micron.

Table 1

Example of layered host crystals susceptible to intercalation by a polymer

Chemical nature	Examples
Element	Graphite [8]
Metal chalcogenides	(PbS) _{1.18} (TiS ₂) ₂ [9], MoS ₂ [10]
Carbon oxides	Graphite oxide [11,12]
Metal phosphates	Zr(HPO ₄) [13]
Clays and layered silicates	Montmorillonite, hectorite, saponite, fluoromica, fluorohectorite, vermiculite, kaolinite, magadiite, ...
Layered double hydroxides	M ₆ Al ₂ (OH) ₁₆ CO ₃ ·nH ₂ O; M=Mg [14], Zn [15]

Intercalazione con polimeri

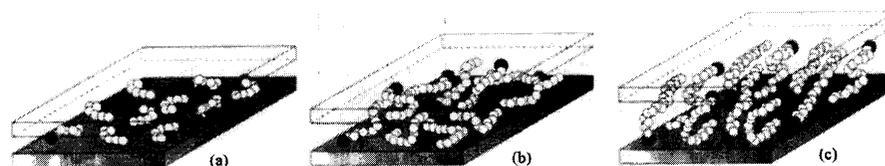
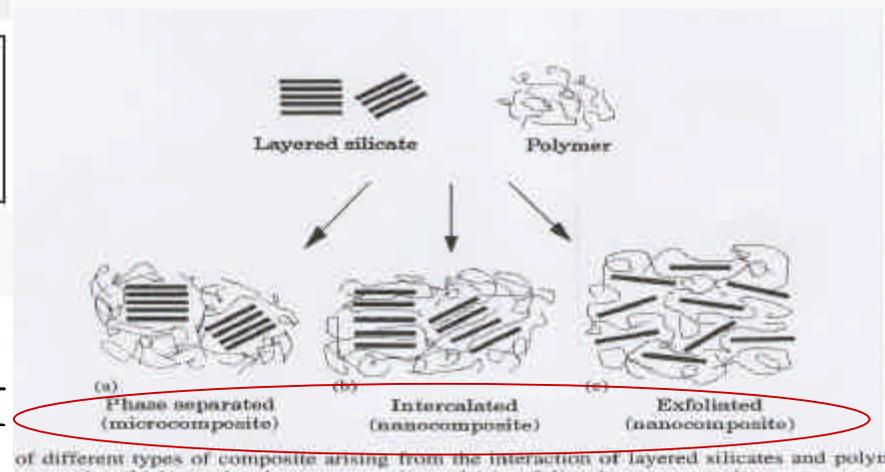


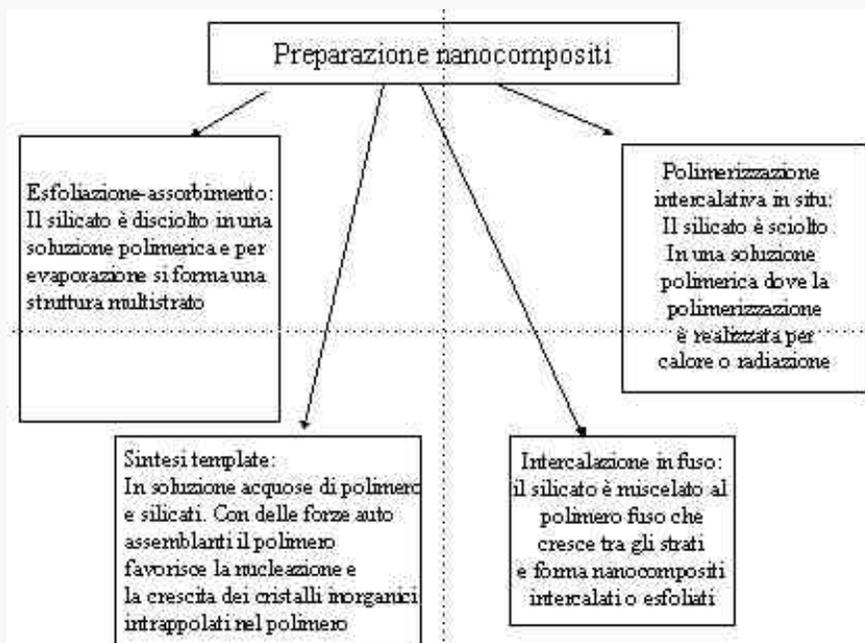
Fig. 3. Alkyl chain aggregation models: (a) short alkyl chains: isolated molecules, lateral monolayer; (b) intermediate chain lengths: in-plane disorder and interdigitation to form quasi bilayers and (c) longer chain length: increased interlayer order, liquid crystalline-type environment (reproduced from [21] with permission).



Host crystals (tipo silicati) intercalati con polimeri:
 varie configurazioni possibili

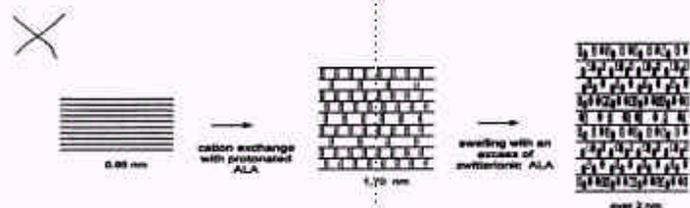
Materiale tratto dal seminario di
 Elio Bibbò, Aprile 2004

Cenni su nanocompositi polimerici II



Polimerizzazione intercalativa in situ

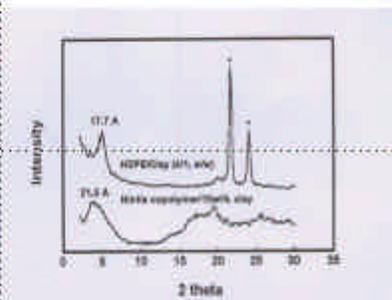
Con tale metodo sono ottenuti nanocompositi di nylon. Tra i più interessanti c'è il nanocomposito del nylon-12 tramite polimerizzazione intercalativa in situ. Per aumentare l'adesione tra le due fasi si è usato l'acido 12-amminolaurico (ALA). In base alla quantità di ALA utilizzato si arriva ad aumentare distanza tra gli strati di silicio e a favorire l'intercalazione del polimero stesso.



Esfolazione-assorbimento

Questa tecnica è usata per polimeri idrosolubili come polivinilalcol, polietileneossido, polivinilpirrolidone o poliacidoacrilico che formano strutture esfoliate.

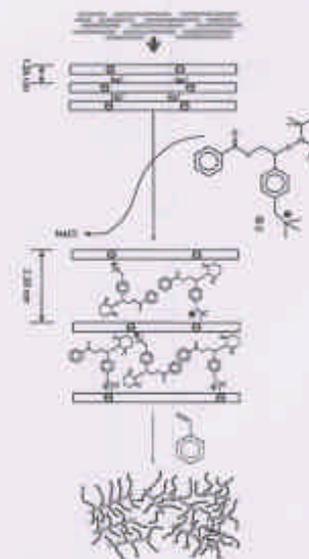
Sono stati realizzati nanocompositi con copolimeri nitrilici o con HDPE



Interessanti film di nanocompositi con PLA e PCL e montmorillonite di sodio con notevoli proprietà fisiche.

Un altro interessante nanocomposito è con polistirene polimerizzato in soluzione con Na-montmorillonite in presenza di cationi organici (scambio cationico) e di iniziatori radicalici per la polimerizzazione del PS.

Per realizzare un'effettiva adesione tra le due fasi si è realizzata la polimerizzazione vivente del PS sulla superficie del fillosilicato, funzionalizzando la montmorillonite con cationi ammonio portanti gruppi nitrossidi che favoriscono la crescita del PS.



Cenni su nanocompositi polimerici III

Proprietà

Gli strati di silicato hanno dimostrato un notevole miglioramento delle proprietà del polimero in cui sono dispersi. Tra queste proprietà un aumento del modulo elastico con un quantitativo circa del 1% in peso del riempitivo inorganico. Stabilità termica, ignifughi con formazione di carbone e delle buone proprietà barriera per i gas e trasmissione di vapore.

Proprietà meccaniche

I nanocompositi nylon-6 ottenuti per polimerizzazione intercalativa di apertura dell'anello di ϵ -caprolattame mostrano un notevole aumento del modulo di Young.

Table 12
Effect of nylon-6-based nanocomposite preparation on the Young's modulus related to the filler content and the average molecular weight of the matrix

Sample preparation	Filler content (wt.%)	MW ($\times 10^3$)	Young's modulus (GPa)
Commercial nylon-6	0	13.0	1.11
NCC ^a	5	13.0	1.06
NCH ^b	4.7	16.3	1.87
1-NCH ^c	5.3	19.7	2.04
one-pot-NCH ^d	4.1	22.6	2.25

^a NCC: montmorillonite-based nylon microcomposite.

^b NCH: nanocomposite obtained by in situ intercalative polymerization of ϵ -caprolactam in protonated aminododecanoic modified montmorillonite [18].

^c 1-NCH: nanocomposite obtained by in situ intercalative polymerization of ϵ -caprolactam in protonated ϵ -caprolactam modified montmorillonite [50].

^d One-pot-NCH: nanocomposite obtained by in situ intercalative polymerization of ϵ -caprolactam with Na-montmorillonite [51].

Eccellenti proprietà meccanico/strutturali legate a natura nanocomposita

Un notevole modulo elastico è stato mostrato anche da nanocompositi elastomerici reticolati in poliuretano che presentano una struttura esfoliata.

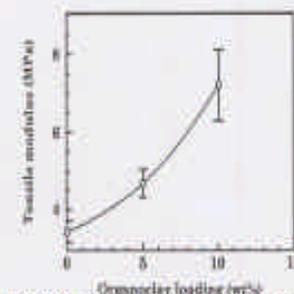
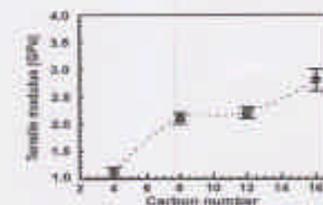


Fig. 10. Translucida modulus for elastomeric polyurethane nanocomposites.

Altre strutture esfoliate con un un notevole modulo elastico sono i nanocompositi epossidici con anmmine vulcanizzate con un 2% in peso di montmorillonite modificata con cationi alchilammonio di varia lunghezza.



Elongazione a rottura

I nanocompositi elastomerici epossidici mostrano una significativa elongazione a rottura. Tali nanocompositi mostrano notevoli proprietà fisiche che ne fanno dei materiali ad alte prestazioni.

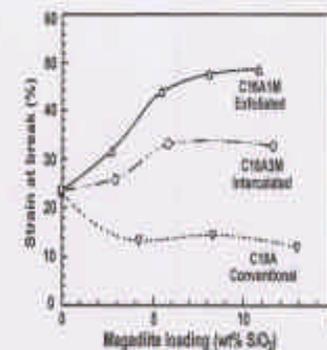


Fig. 11. Strain at break values for an exfoliated epoxy/nanofiller nanocomposite.